

January 2012

Implementation and Optimization of an Inverse Photoemission Spectroscopy Setup

Ervin Gina

University of South Florida, ervin.gina@gmail.com

Follow this and additional works at: <http://scholarcommons.usf.edu/etd>

 Part of the [American Studies Commons](#), [Electrical and Computer Engineering Commons](#), and the [Materials Science and Engineering Commons](#)

Scholar Commons Citation

Gina, Ervin, "Implementation and Optimization of an Inverse Photoemission Spectroscopy Setup" (2012). *Graduate Theses and Dissertations*.

<http://scholarcommons.usf.edu/etd/4050>

This Thesis is brought to you for free and open access by the Graduate School at Scholar Commons. It has been accepted for inclusion in Graduate Theses and Dissertations by an authorized administrator of Scholar Commons. For more information, please contact scholarcommons@usf.edu.

Implementation and Optimization of an Inverse Photoemission Spectroscopy Setup

by

Ervin Gina

A thesis submitted in partial fulfillment
of the requirements for the degree of
Master of Science in Electrical Engineering
Department of Electrical Engineering
College of Engineering
University of South Florida

Major Professor: Rudy Schlaf, Ph.D.
Arash Takshi, Ph.D.
Jing Wang, Ph.D.

Date of Approval:
June 8, 2012

Keywords: Unoccupied Electron States, Conduction Band Minimum,
Transfer Gap Analysis, Photon Detection, Isochromat Mode

Copyright © 2012, Ervin Gina

DEDICATION

This thesis is dedicated to my family for their support and encouragement over the years. I am extremely grateful to my parents for always putting my education first and instilling in me a desire for knowledge and a drive to always better myself.

ACKNOWLEDGMENTS

First and foremost, I would like to express my sincere gratitude to Dr. Schlaf, who has supervised the work required for this thesis. I am grateful for his guidance and support. Furthermore, I am thankful to the members of my committee for providing advice on how to improve my work.

I would like to thank Matthaus Wolak for his invaluable assistance in the laboratory and our discussions regarding PES and IPES. I would also like to thank all other past and present members of the Surface Science Laboratory at the University of South Florida, especially Jan Alsmeier for his help with the setup and Michael Schaefer for his assistance in editing.

Finally, I would like to express my appreciation to my girlfriend Stella Kratzer for her support and understanding during my master's work. There were difficult times during this study where her encouragement helped me push through.

TABLE OF CONTENTS

LIST OF TABLES	iii
LIST OF FIGURES	iv
ABSTRACT.....	vii
CHAPTER 1: INTRODUCTION AND FUNDAMENTALS.....	1
1.1 Motivation and Objective	1
1.2 Overview.....	2
1.3 Photoelectric Effect	3
1.4 Photoemission Spectroscopy (PES)	4
1.5 Inverse Photoemission Spectroscopy (IPES)	9
1.6 Photon Proportional Counter.....	15
1.7 Electron Gun Theory.....	17
CHAPTER 2: EXPERIMENTAL METHODOLOGY	20
2.1 Experimental Setup	20
2.1.1 Integrated Surface Science System	20
2.1.2 Sample Preparation	21
2.2 IPES instrumentation.....	22
2.2.1 Electron Gun and Power Supply	22
2.2.2 Photon Detector	23
2.2.3 Gas Manifold	24
2.2.4 Counter Electronics.....	26
2.3 LabVIEW Software	28
2.3.1 Manual Mode	28
2.3.2 Automatic Mode	30
2.3.3 Detector Voltage Scan	31
CHAPTER 3: PHOTON DETECTOR OPERATION AND TESTING	33
3.1 Proportional Counter Gas and Window Selection	33
3.2 Acetone Purification.....	36
3.3 Pressure Testing.....	38
CHAPTER 4: SOFTWARE AND ELECTRONICS	44
4.1 Electronics Operation Test	44
4.2 Electron Gun LabVIEW Interface	46

4.3 IPES LabVIEW Software.....	48
4.3.1 NI DAQmx.....	48
4.3.2 Sample Current Reading.....	50
4.3.3 Stanford Power Supply Control.....	52
4.3.4 “Automatic Mode” Flowchart	53
4.3.5 Data Acquisition.....	55
CHAPTER 5: EXPERIMENTAL IPES SCANS AND CONCLUSION.....	61
5.1 Experimental Resolution of Detector.....	61
5.2 IPES Scan of Indium Tin Oxide (ITO).....	63
5.3 Conclusion.....	65
REFERENCES	66
APPENDICES	70
Appendix A: Filling the Detector with Gas.....	71
Appendix B: Starting Up the Electron Gun.....	73
Appendix C: Setting Up Electronics.....	75
Appendix D: Starting a Measurement	77
Appendix E: Copyright Permissions	82

LIST OF TABLES

Table 1: Window element cutoff energy comparison.....	33
Table 2: The count rate vs. applied voltage for 3.1 mbar (N ₂) acetone pressure is shown.	39

LIST OF FIGURES

Figure 1: Inverse photoemission spectroscopy setup schematic overview.....	3
Figure 2: Universal curve of electron mean free path as a function of an electron's energy.....	6
Figure 3: Photoemission spectroscopy energy transference.	7
Figure 4: UPS scan of sputtered and unsputtered anatase TiO ₂	9
Figure 5: Inverse photoemission spectroscopy energy transference.....	11
Figure 6: IPES measurement and comparison to literature of Ag and Ta by Shukla et al.....	13
Figure 7: Surface and interface states for Bi overlaid on GaAs.....	14
Figure 8: Photon detector cutout showing ionization of atoms.	16
Figure 9: Electron gun block diagram.	19
Figure 10: Integrated surface science system.	21
Figure 11: Kimball Physics EGPS-1022 power supply.....	22
Figure 12: Electrical feedthrough and anode.	23
Figure 13: Feedthrough connected to CaF ₂ viewport.	24
Figure 14: Gas manifold system for pumping and filling detector.....	25
Figure 15: Manual mode for IPES measurement at a fixed electron energy.....	29
Figure 16: Automatic mode for scanning a spectrum of unoccupied states in a material by varying incident electron energy.....	31

Figure 17: Detector voltage scan utilized when determining an optimum applied high voltage between anode and cathode.....	32
Figure 18: Acetone photoionization cutoff plot.....	34
Figure 19: Overlap of acetone photoionization and CaF ₂ transmission for the optical bandpass.....	35
Figure 20: Frozen acetone while evacuating the vial.....	37
Figure 21: Count rate vs. applied high voltage for a fixed energy above the Fermi edge (1 mbar acetone / 200 mbar acetone and argon gas mixture).....	40
Figure 22: Count rate vs. applied high voltage for a fixed energy above the Fermi edge (varied gas mixtures).....	41
Figure 23: The various gas mixtures were used to scan Au from 2-14 eV and the intensity deviation has been plotted via the variation in each scan.	43
Figure 24: A square wave pulse is fed into the test input of the preamplifier (Channel 2).....	44
Figure 25: The output of the amplifier (Channel 1).....	45
Figure 26: The 5 V output of the signal channel analyzer (Channel 1).....	46
Figure 27: Electron gun LabVIEW interface created by Kimball Physics.	47
Figure 28: IPES software data binding to local "step" variable.....	48
Figure 29: National Instruments DAQmx task to read counts.....	49
Figure 30: Sample current acquisition setup.....	50
Figure 31: LabVIEW stage current reading and averaging.	51
Figure 32: Sample current front VI display.	51
Figure 33: Stanford PS-350 LabVIEW control loop.	52
Figure 34: Automatic mode flowchart.....	54
Figure 35: Count rate array creation.	56
Figure 36: Counting loop for each individual step measurement.	57

Figure 37: Energy step increase structure.	58
Figure 38: Array build for final output that is saved to .xy file.	59
Figure 39: Sample output .xy data file.	60
Figure 40: Sputtered Au measurement used to determine resolution of system.	62
Figure 41: IPES scan of Au.	63
Figure 42: IPES scan of ITO showing a shift in the conduction band.	64
Figure 43: Electron gun cathode temperature vs. current.	74
Figure 44: a) The preamplifier, b) amplifier and c) single channel analyzer component images.	76

ABSTRACT

Inverse photoemission spectroscopy (IPES) is utilized for determining the unoccupied electron states of materials. It is a complementary technique to the widely used photoemission spectroscopy (PES) as it analyzes what PES cannot, the states above the Fermi energy. This method is essential to investigating the structure of a solid and its states. IPES has a broad range of uses and is only recently being utilized.

This thesis describes the setup, calibration and operation of an IPES experiment. The IPES setup consists of an electron gun which emits electrons towards a sample, where photons are released, which are measured in isochromat mode via a photon detector of a set energy bandwidth. By varying the electron energy at the source, a spectrum of the unoccupied density of states can be obtained. Since IPES is not commonly commercially available the design consists of many custom made components. The photon detector operates as a bandpass filter with a mixture of acetone/argon and a CaF_2 window setting the cutoff energies. The counter electronics consist of a pre-amplifier, amplifier and analyzer to detect the count rate at each energy level above the Fermi energy.

Along with designing the hardware components, a Labview program was written to capture and log the data for further analysis. The software features several operating modes including automated scanning which allows the user to enter the desired scan parameters and the program will scan the sample accordingly. Also implemented in the

program is the control of various external components such as the electron gun and high voltage power supply.

The new setup was tested for different gas mixtures and an optimum ratio was determined. Subsequently, IPES scans of several sample materials were performed for testing and optimization. A scan of Au was utilized for the determination of the Fermi edge energy and for comparison to literature spectra. The Fermi edge energy was then used in a measurement of indium tin oxide (ITO) determining the conduction band onset. This allowed the determination of the “transfer gap” of ITO. Future experiments will allow further application of IPES on materials and interfaces where characterization of their electronic structure is desired.

CHAPTER 1: INTRODUCTION AND FUNDAMENTALS

1.1 Motivation and Objective

Photoemission spectroscopy (PES) has been widely implemented as an essential tool for characterizing the electronic structure of a material but it is limited as it only measures the occupied electron states below the Fermi edge energy. To quantify the complete structure including the conduction band minimum (CBM) one had to previously estimate the location of the CBM using theoretical data or optical band gap analysis. However, there is a need to determine the transfer gap of a material for analyzing the conduction band onset and unoccupied states. Inverse photoemission spectroscopy (IPES) is one such method that can probe the unoccupied states above the Fermi edge energy including the CBM. When IPES is used in conjunction with PES, the electron and hole injection barriers can be characterized as well as other electrical properties.

The objective of this thesis is to detail the implementation and optimization of an inverse photoemission spectroscopy setup whose future analysis application will cover a wide range of materials and interfaces. Additionally, this thesis will also serve as a reference manual for all surface science lab members when analyzing materials using the IPES setup. The design of the IPES system has been modeled after several published setups. The IPES components include an electron source, photon detector, high voltage

power supply, counter electronics and computer. In order to analyze the data from the IPES setup a LabVIEW program was created to capture and log data.

After assembly of the IPES setup the system was characterized with sample materials. Operating parameters were obtained for scanning and the analyzer broadening was investigated by scanning a metallic sample and measuring the width of the Fermi edge energy slope. Lastly, tin doped indium oxide was analyzed as an example to show transfer gap analysis with IPES using previously published valence band maximum (VBM) data.

1.2 Overview

A schematic of the IPES setup implemented in this thesis is shown in Figure 1. An electron source is directed at a sample where the electrons couple to unoccupied states within the material and radiate energy in the form of photons. The photons are then quantified using a bandpass detector where the detected current pulse is fed through a series of components such as the preamplifier to convert the current pulse to a voltage pulse, an amplifier to shape the signal and a single channel analyzer where counts are separated from the noise of the system. The counts exiting the single channel analyzer are fed into the computer where the custom LabVIEW program logs the data. The sample current is read with a picoammeter and is also input to the LabVIEW program.

There are two methods for obtaining a spectrum of the unoccupied states, isochromat and spectrograph modes. Isochromat scanning involves varying the incident electron energy while using a constant detected photon energy to plot states above the

Fermi edge energy. Spectrograph scanning works similarly but differs where the incident electron energy is kept fixed and the detected photon energy is varied with a grating spectrometer. The former method is utilized in this IPES setup due to lower implementation costs and ease of maintenance.

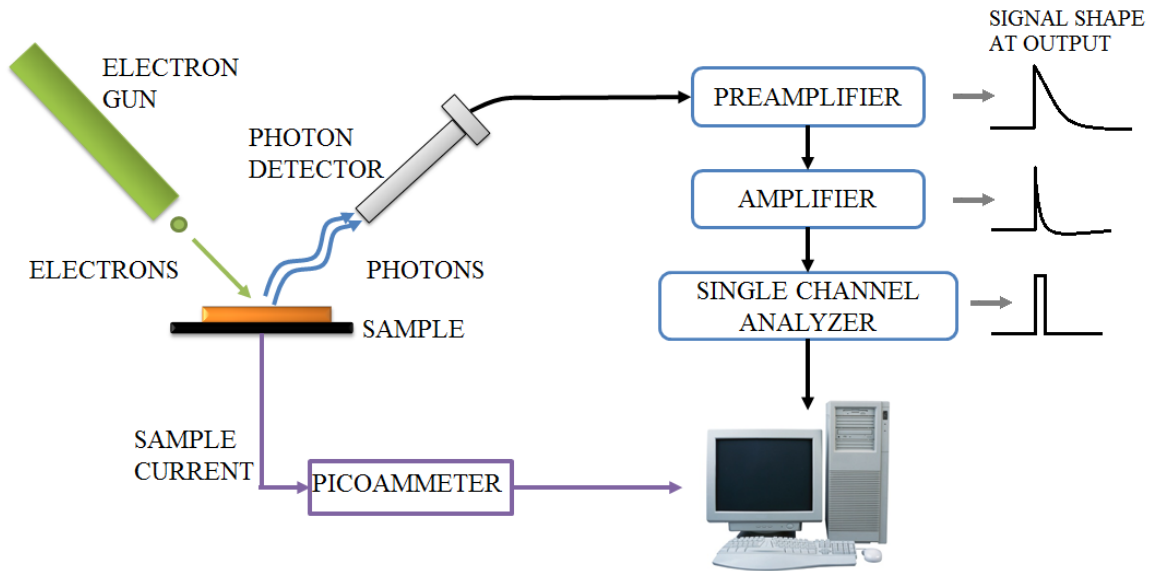


Figure 1: Inverse photoemission spectroscopy setup schematic overview.

1.3 Photoelectric Effect

Photoemission and inverse photoemission spectroscopy are used to measure different bands of a material and are inverses of one another. However, both are based on the photoelectric effect first observed by Heinrich Hertz in 1887 [1]. Hertz observed that the required voltage to induce sparks in a gap was reduced when he introduced UV light. In 1905 it was Einstein though who explained the photoelectric effect in solids. The energy of a photon E is related to its frequency ν and Planck's constant h by [2, 3]:

$$E = h \times \nu. \quad \text{Equation 1}$$

This energy can be transferred to an electron in photoemission spectroscopy. Einstein predicted the maximum kinetic energy of an electron released from a solid to be [4]:

$$E_{kin}^{max} = h\nu - \phi, \quad \text{Equation 2}$$

where ϕ is referred to as the *work function* of the solid and is the minimum energy required to remove an electron from the surface to vacuum.

1.4 Photoemission Spectroscopy (PES)

Photoemission spectroscopy is one of the most widespread methods for analyzing the electronic structure of solids and surfaces [5]. A monochromatized light source generates photons directed at a sample. Energy is then transferred to electrons that will leave the sample and their E_{kin} is measured with an analyzer. It was in the 1960's when photoemission spectroscopy started to become an indispensable tool to measure chemical and electronic properties of a material. The first ultraviolet photoemission spectroscopy (UPS) valence band spectrum was measured on copper in 1963 by Spicer et al. [6]. The benefit of photoemission spectroscopy, both ultraviolet and x-ray, is the wealth of information that can be obtained from characterizing a material with these methods. Some of the parameters include frequency, polarization, angle of incidence, crystal face and surface structure and the spin polarization of electrons [7]. Knowledge of PES is crucial to understanding the theory of IPES. Therefore a solid background regarding PES will first be introduced.

The initial difficulty with PES stemmed from the need of stringent vacuum conditions. In recent times Ultra-High Vacuum (UHV) conditions are easier to obtain. Additionally, the investigation of the surface states of a material requires a clean surface. High surface sensitivity results from the short inelastic mean free path of electrons in matter, which is defined as the average distance the electrons can travel between collisions [8]. It determines the depth of the sample available to be analyzed even though photons can penetrate to depths of tens of μm . Electrons on the surface have a lower probability of scattering at atoms and therefore are more likely to escape the sample. If the sample surface is not clean, electrons are absorbed by the contamination layer. This impairs the characterization of the sample. The inelastic mean free path λ is given by Tanuma et al. [9] as:

$$\lambda = E / (E_p)^2 \left[\beta \ln(\gamma E) - \left(\frac{C}{E} \right) + \left(\frac{D}{E^2} \right) \right], \quad \text{Equation 3}$$

- E = electron kinetic energy (eV)
- E_p = free electron plasmon energy [$28.8 (N_v \rho / M)^{1/2}$]
- ρ = density (g/cm^3)
- N_v = number of valence electrons per atom or molecule
- M, β, γ, C, D = atomic or molecular weight parameters.

By examining many different elements such as aluminum, gold, iron, mercury and tungsten, Tanuma et al. were able to determine empirical values for the atomic and molecular weight parameters. Independent of particular materials properties the mean free path usually follows a curve as shown in Figure 2.

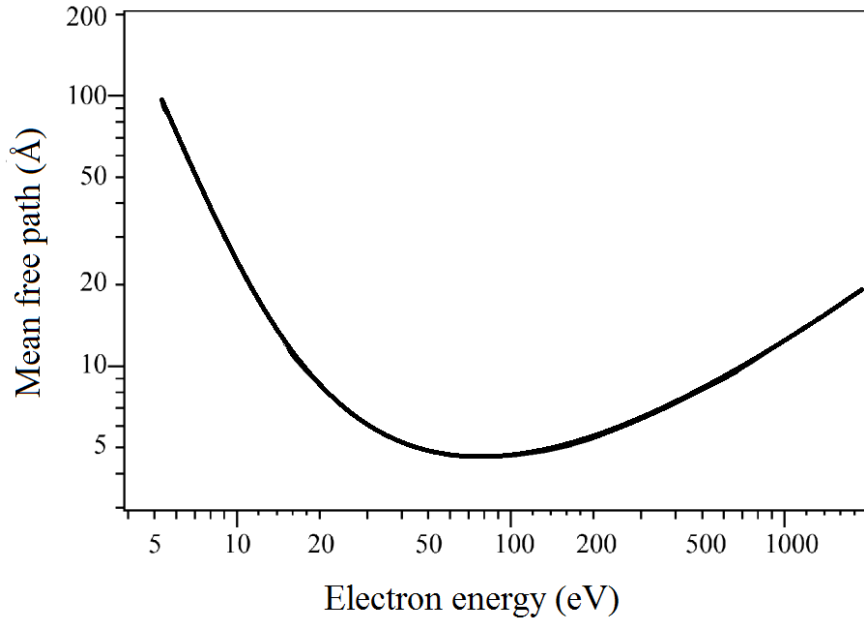


Figure 2: Universal curve of electron mean free path as a function of an electron's energy. [10]

The PES process is usually described with a three-step model. First, the photoionization occurs and the photon energy excites an electron. Second, the aforementioned electron is transported to the surface of the solid. Third, the excited electron penetrates through the surface and enters the vacuum. This separation of stages does not exist in reality but it helps analyzing this process [11].

The energy levels below the Fermi energy are occupied states and can be quantized with PES. The data gathered from PES can directly show the density of states and the work function of a sample. Figure 3 illustrates the energy conversion diagram related to PES. The following equation describes the transfer of energy from the initial photon and the final kinetic energy that is expected:

$$E_{kin} = h\nu - E_b - \phi. \quad \text{Equation 4}$$

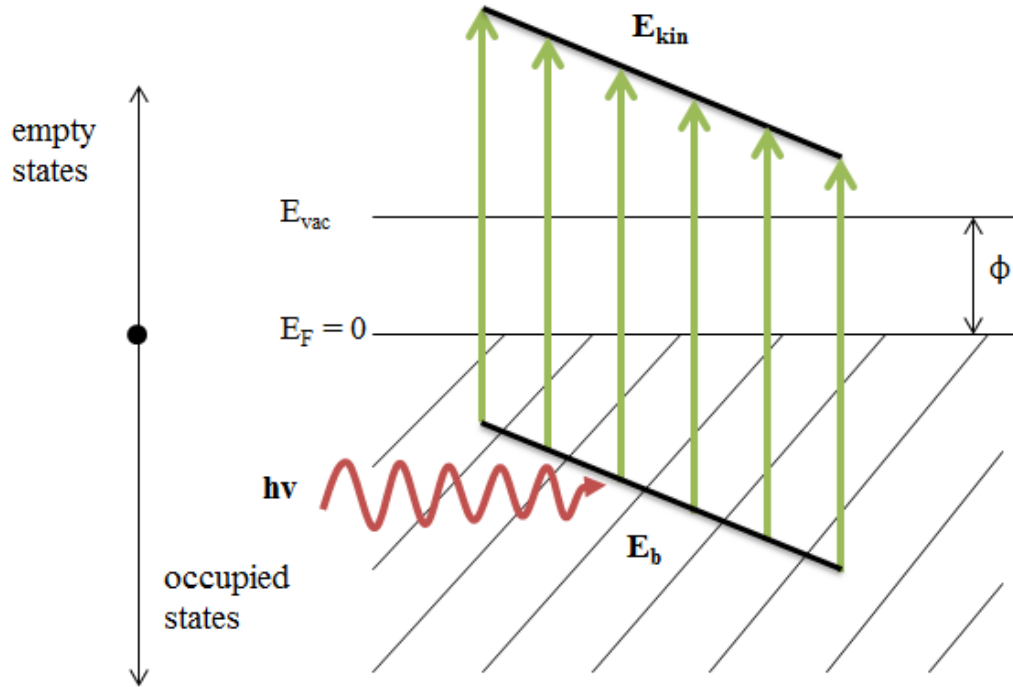


Figure 3: Photoemission spectroscopy energy transference.

The binding energy E_b of an electron is given relative to the Fermi energy, $E_F = 0$. For a constant photon energy and a metallic sample, electrons with the highest measured kinetic energy will originate from the Fermi energy where their binding energy is 0 and $E_{kin} = h\nu - \phi$. The lowest kinetic energy electrons to leave the sample will have barely enough energy to stay in vacuum. This energy represents the work function of the material. In this case, $h\nu \approx E_b + \phi$ so $E_{kin} \approx 0$ [12]. The momentum ρ of the ejected electron is related to its kinetic energy by:

$$E_{kin} = \frac{\rho^2}{2m}, \quad \text{Equation 5}$$

which can be written as:

$$\rho = \sqrt{2mE_{kin}}, \quad \text{Equation 6}$$

with the electron mass m .

For core level emissions x-ray photoemission spectroscopy (XPS) is utilized. The energy of the core levels is element-specific, i.e. XPS can be used to measure the stoichiometry of a sample. The chemical interaction between atoms is revealed through peak shifts of the core level lines.

By using UPS, information about the valence states can be obtained. XPS can also probe the valence states but is not utilized due to the lower resolution. UPS features a resolution of 200 meV while XPS is limited to 200 - 900 meV depending on the line width of the exciting light. The photon source for UPS is usually a helium gas discharge lamp where the He I and He II lines are used at 21.21 eV and 40.6 eV. From Figure 2 it is apparent that the inelastic mean free path is lower for UPS which implies increased surface sensitivity when compared to XPS.

UPS directly yields the valence bands density of states (DOS) of the sample surface. Information about the band structure and other properties such as band offsets at materials interfaces can also be obtained. It is of importance to note PES is a final state energy measurement where the measured energies correspond to the ionized state of the investigated material.

Figure 4 is an example of a UPS measurement on a TiO₂ sample. The valence band emissions are approximately between the binding energies of 4 to 8 eV. This emission is proportionally related to the density of states and allows the measuring of the valence band maximum (VBM) which is crucial in addition to IPES in determining the transfer gap of a material. The work function of the material can also be deduced by

investigating the secondary electron onset which in this measurement is around 17 eV and subtracting this value from the excitation energy of 21.2 eV [13]. The onset originates from the scattered secondary electrons that contain the minimum energy required to escape the surface.

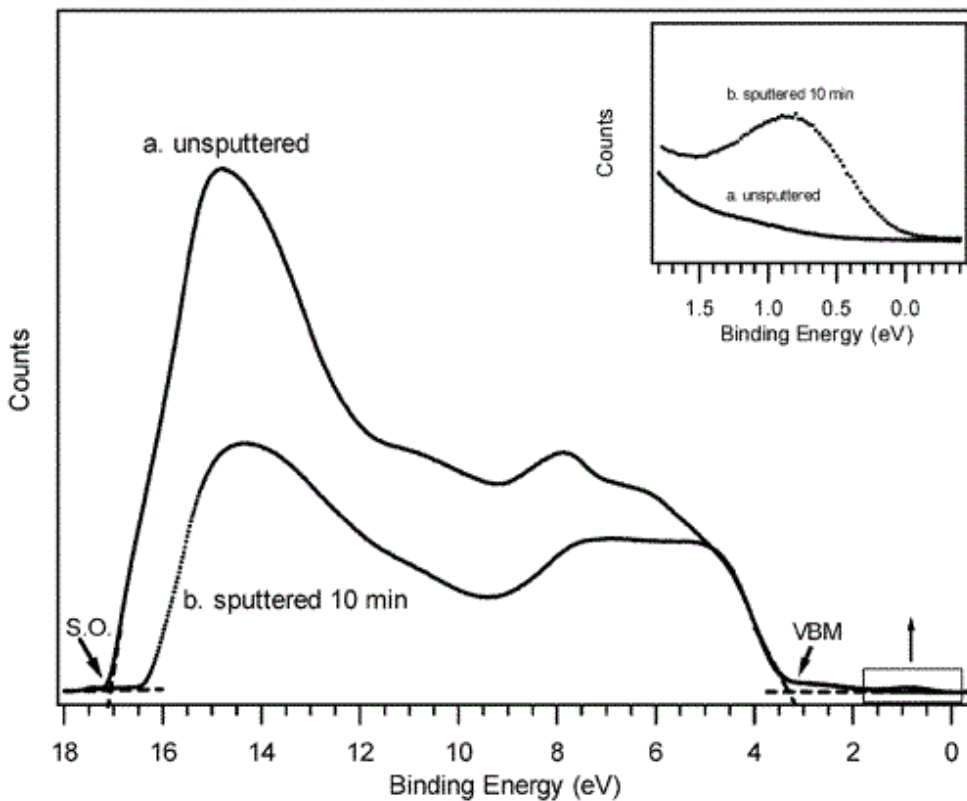


Figure 4: UPS scan of sputtered and unspattered anatase TiO₂. Reprinted (adapted) with permission from ([13]). Copyright 2012 American Chemical Society.

1.5 Inverse Photoemission Spectroscopy (IPES)

IPES allows the probing of the unoccupied states of a sample. The electron gun emits monochromatic electrons to a sample where they couple to unoccupied electron

states. Photons resulting from the radiative decay into lower energy states can be measured. These outgoing photons are measured with a proportional counter acting as a bandpass detector consisting of a CaF_2 window setting the low pass filter and an ionizing gas (acetone) defining the high pass filter. The constant energy detection set by the fixed window designates the setup as isochromat spectroscopy [14].

Inverse photoemission spectroscopy has always lagged behind photoemission spectroscopy in respect to development. In 1895 x-rays were discovered by Roentgen [15]. Although Einstein described the photoelectric effect in 1905 it was not until 1915 that the first experiment confirmed the inverse of that theory by Duane and Hunt [16]. They reported the minimum X-ray wavelength emitted from a sample that is under bombardment of electrons. This was the beginning of what today is called inverse photoemission spectroscopy.

Transfer of energy in IPES can be described as the difference in the initial kinetic energy of the electron to the final photon state:

$$h\nu = E_i - E_f. \quad \text{Equation 7}$$

Similar to PES, an inverted three-step model is used to describe the IPES process. First an electron of known energy impinges on the sample and couples to an unoccupied state above the Fermi edge energy. In the second step the electron decays. Decaying occurs either radiatively, where a photon is released, or non-radiatively where the energy is lost through inelastic collisions. The emitted photons are measured via the photon detector [17].

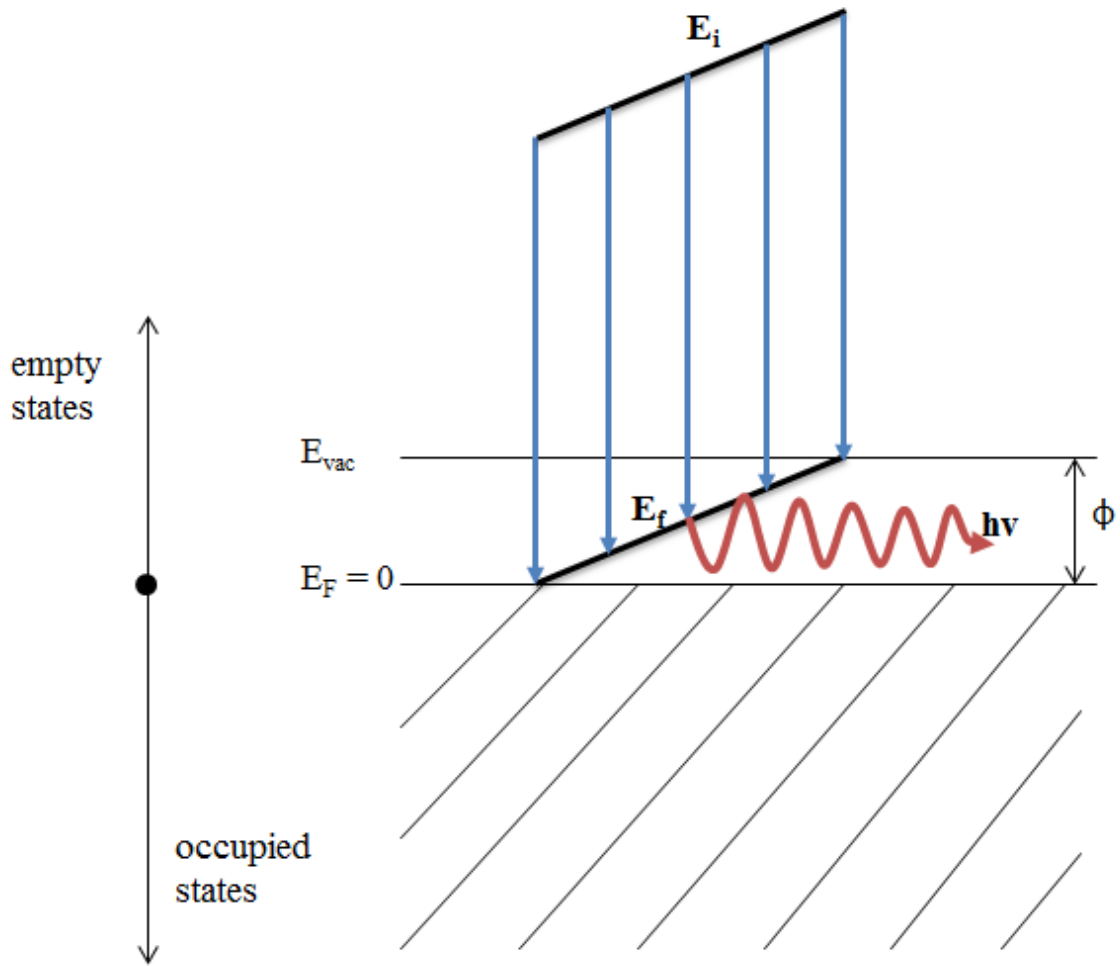


Figure 5: Inverse photoemission spectroscopy energy transference.

IPES in comparison to PES possesses a much lower output of photons vs. electrons in the final state. The wavelength of the photons is substantially longer than electrons with comparable energy resulting in a lower cross section [18, 19]. The cross section describes the probability of interaction between particles. The emission cross section of IPES is further reduced about 10^{-8} photons per electron due to the phase factor, which is inversely proportional to the wavelength of the emitted light [20]. The ratio of the cross section between IPES and PES is found to be [21]:

$$\frac{\sigma_{IPES}}{\sigma_{PES}} \approx \left(\frac{\lambda_{el}}{\lambda_{ph}} \right)^2 = \frac{E_{ph}^2}{2 \times m_{el} \times c^2 \times E_{el}} = \alpha^2 \times \frac{\left(\frac{E_{ph}}{R} \right)^2}{4 \times \left(\frac{E_{el}}{R} \right)}, \quad \text{Equation 8}$$

λ_{el} = wavelength of the electron

λ_{ph} = wavelength of the photon

E_{ph} = photon energy

E_{el} = electron energy (kinetic)

m_{el} = electron mass

R = Rydberg constant ≈ 13.6057 eV

α = $\frac{k_e \cdot e^2}{\hbar \cdot c} \approx 7.2974 \times 10^{-3}$.

Surface sensitivity in IPES is of concern. From Figure 2 it can be seen that the mean free path for the range of electrons impinging the sample is marginally larger than UPS. The measurement is strongly affected by adsorption of contaminants on the surface.

The unoccupied density of states is obtained from IPES measurements. Figure 6 illustrates IPES data for two metals, silver and tantalum [22]. From these scans the energy of the conduction band minimum (CBM) can be obtained. As will be shown in Chapter 5, this data is used to determine the conduction band shifts of other materials with respect to the Fermi edge E_F . When used in conjunction with the PES VBM, the transfer gap can be quantified.

The transfer gap, determined from PES and IPES, is a measurement of the energy required to create an uncorrelated free electron and hole whereas the optical band gap, determined with UV-Vis absorption, refers to the onset creation of an exciton. Therefore the optical gap is smaller than the transfer gap by a significant amount. The binding

energy E_b required in an exciton to break the electron-hole pair has been determined through experimental and theoretical techniques to be approximately 0.5 - 1.5 eV in a molecular solid, 0.2 – 0.5 eV in polymers and ~ 10 meV in inorganic solids [23].

Aside from measurements of metal surfaces also semiconducting and molecular materials can be measured. Furthermore, interfaces such as metal-metal, metal-semiconductor and semiconductor-semiconductor can be characterized. This allows the measurement of electron injection barriers and other semiconductor structures.

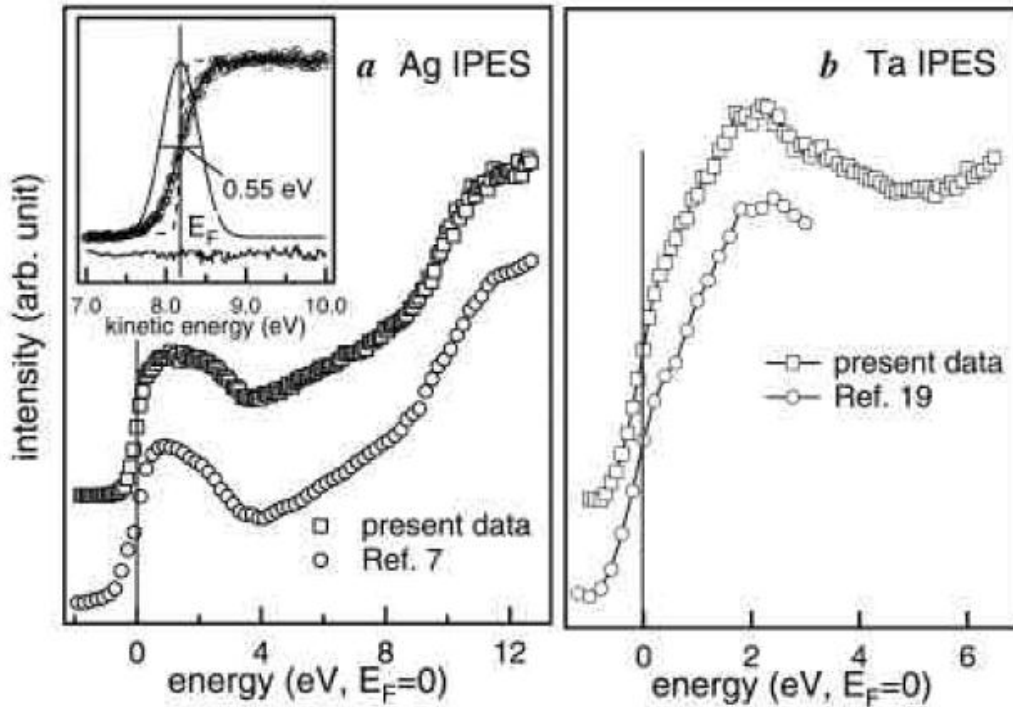


Figure 6: IPES measurement and comparison to literature of Ag and Ta by Shukla et al. Reprinted with permission [22].

Figure 7 shows an example of a metal-semiconductor interface measurement. Here the group V element bismuth is overlaid on the surface of gallium arsenide. The clean measurement of GaAs is shown alongside the bottom of the figure and features a

surface state at around 2 eV relative to the VBM. This measurement example is particularly interesting considering that the change of the states can be visualized as the layers were added. The first layer appears just below 2 eV and by 1.0 ML growth one can see the emergence of the second layer. Each additional layer decreases the transfer gap. The new interface state shows the bonding of Bi-Ga and Bi-As [21]. An image state is also shown in the figure stemming from the long-range image potential near the vacuum level.

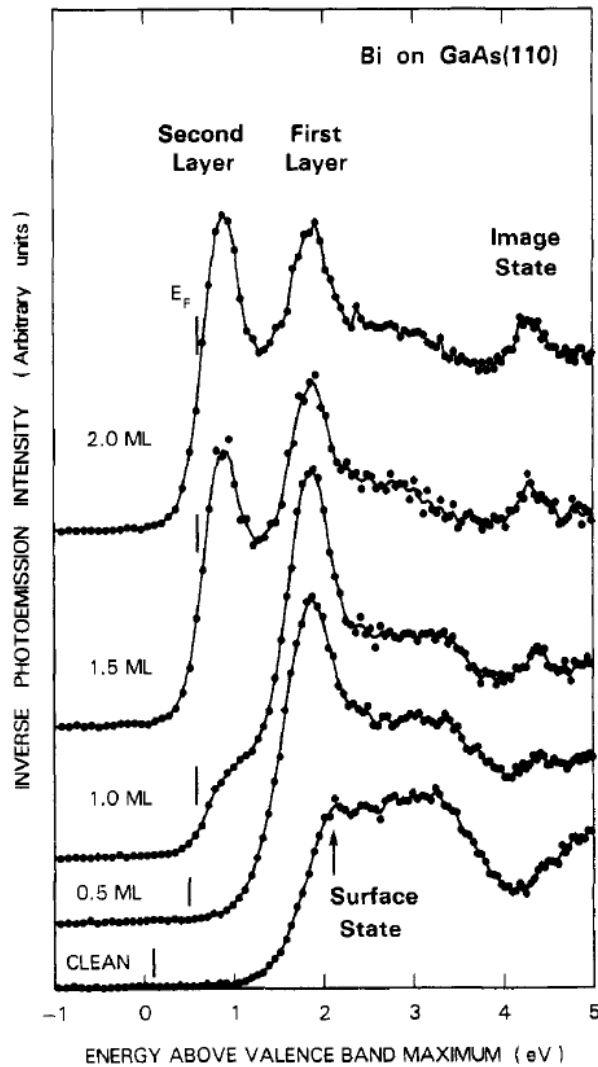


Figure 7: Surface and interface states for Bi overlaid on GaAs. [21]

1.6 Photon Proportional Counter

IPES requires the ability to detect emitted photons from the sample as electrons fill the unoccupied states. The most common detector used is a gas-filled counter referred to as a Geiger-Mueller tube which was developed for the detection of ionizing radiation [24]. The Geiger-Mueller tube was initially utilized to detect high energy alpha, beta and gamma radiation. It was first used specifically for IPES by Denninger et al. [25, 26]. The typical counter is an end-window type with a filtering material to filter the energy of the incoming radiation. The same counter can be operated in different modes where the applied high voltage between the cathode and anode indicates the region of operation [27]. Going from low to high voltage the counter can behave as an ionization chamber, proportional counter, and Geiger counter. It was shown by Shukla et al. [22] that the proportional counter condition can be used for IPES.

Geiger counters are constructed with a cylindrical cathode tube encapsulating a thin anode wire running through the center. In order to have gas multiplication the applied electric field must be sufficiently high. The electric field $\varepsilon(r)$ at a radius r is given by:

$$\varepsilon(r) = \frac{V}{r \ln\left(\frac{b}{a}\right)}, \quad \text{Equation 9}$$

- V = voltage applied between anode and cathode
- a = anode wire radius
- b = cathode inner radius.

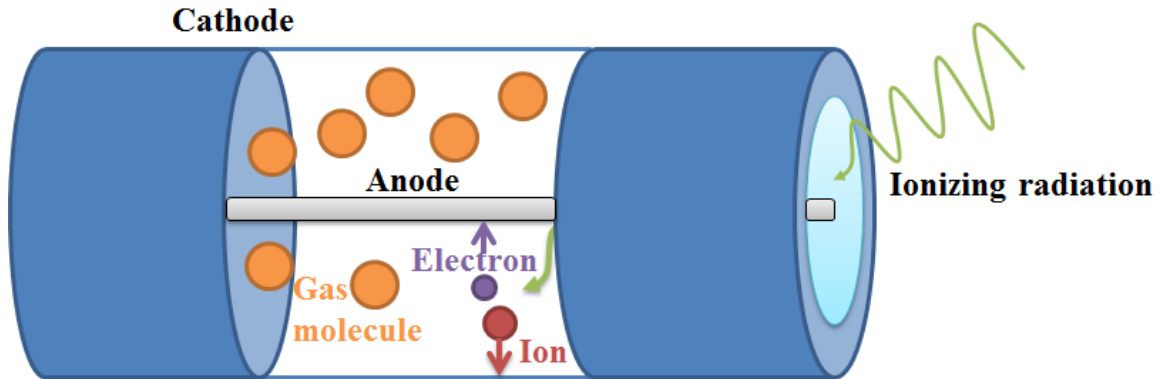


Figure 8: Photon detector cutout showing ionization of atoms.

Single ion pair creation cannot be easily detected as a pulse due to the very small associated current. Typically a gas multiplier is used in conjunction with the ionization gas to amplify the current pulse detected on the anode [28]. This multiplier gas is let into the detector simultaneously along with the ionized gas. The initial electrons accelerated towards the anode through the applied electric field will impact the multiplier gas molecules and eject secondary electrons. This avalanche results in a current pulse that is proportional to the initial ion pair creation, but of much higher magnitude. The multiplier gas cannot have a lower ionization energy than the low pass component of the filter, which in this case is the window affixed to the cathode [29].

Photons with an energy below the window cutoff will enter the photon detector and ionize the gas molecules if their energy exceeds the gas ionization threshold. Depending on the selection of the window and gas, a bandpass is achieved, defining the resolution of the measurement. Variations of window/gas combinations will be discussed later in experimental Chapter 3. Once a molecule is ionized the electron is accelerated towards the anode. The electron then has enough energy to free more electrons from the

multiplier gas it encounters on the way to the anode. The ionized gasses will drift towards the cathode where they get neutralized and so become again ready for ionization.

1.7 Electron Gun Theory

An electron gun suitable for IPES must operate in the single digit eV region, have a reasonably high current, and be focused into a small spot on the sample [17]. Shown in Figure 9 is the block diagram of a refractory metal cathode electron gun.

At temperatures above absolute zero there are electrons that can leave a cathode surface. As the temperature is increased, the number of electrons with enough energy to escape increases. Emission of electrons from a surface by heating is referred to as thermionic emission [30]. The metal cathode is directly heated by a voltage source. When the cathode temperature is relatively low and the 1st anode voltage is high, the cathode operates in a temperature limited mode [31]. In this region an exponential relationship exists between the electron emission and cathode temperature. This is described by the Richardson-Dushman equation:

$$J = AT^2 e^{\frac{-\phi}{kT}}, \quad \text{Equation 10}$$

- J = emission current density (A/cm²)
- A = Richardson's constant for cathode material (A/[cm²*K²])
- T = cathode temperature (K)
- ϕ = work function of cathode (eV)
- k = Boltzmann's constant (8.6 x 10⁻⁵ eV/K).

Operating an electron gun in the temperature limited mode results in the beam current shifting as the temperature drifts. By increasing the cathode temperature and reducing the 1st anode voltage, the cathode then operates in a space charge limited mode. The relationship is described by the Langmuir-Child space charge equation [32]:

$$J = \frac{2.335 \times 10^{-6} x V^{\frac{3}{2}}}{d^2}, \quad \text{Equation 11}$$

- J = emission current density (A/cm²)
- V = cathode to anode voltage difference (V)
- d = distance between cathode and anode (cm).

When the cathode is in the space charge limited region the emission current is fairly steady for changes in temperatures but this results in much shorter cathode lifetimes due to the cathode material evaporating rapidly with higher temperatures [31]. Hence guns are usually operated between the two regions. This provides beam stability and sufficient emission current while maximizing the cathode lifetime [32].

The electron source voltage V_{ES} in Figure 9 is the source of energy for thermionic emission. Once the electrons exit the source they are focused via a series of lenses. The grid voltage V_G can be used to turn off the beam. If the applied grid voltage is negative enough in relation to the cathode it will completely suppress the emission of electrons. This technique can be extended to pulsing the flow of electrons with a relatively fast cycle. The 1st anode lens is used to accelerate the electrons, while focusing occurs in the focus lens controlled by voltage V_F . The beam can be directed in 2 dimensions using a four-pole deflection plate system. Deflection in the x-axis is controlled with V_{XD} whereas deflection in the y-axis is controlled with V_{YD} [32].

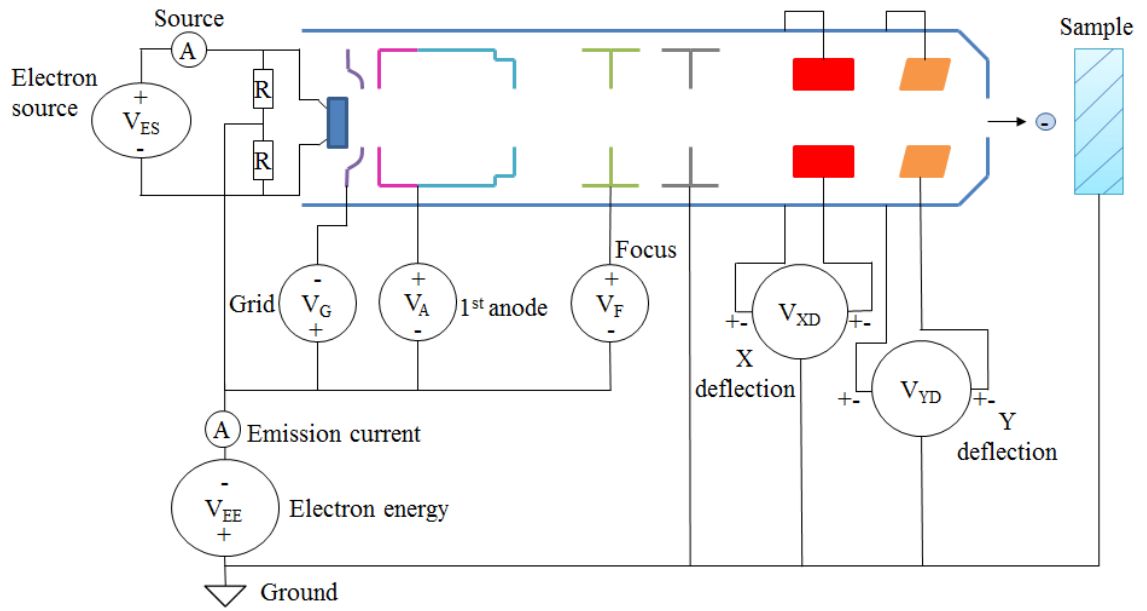


Figure 9: Electron gun block diagram. [32]

CHAPTER 2: EXPERIMENTAL METHODOLOGY

2.1 Experimental Setup

2.1.1 Integrated Surface Science System

The experiments were performed in an integrated high vacuum surface science system. The three chambers are connected via an in situ sample transfer mechanism allowing transfer without exposing a sample to atmosphere. The base pressure of the system was at 5×10^{-10} mbar. The sample is loaded via the fast entry load lock and from there can be transferred into any chamber according to deposition or analysis needs. Each chamber is isolated with gate valves unless transferring a sample. Inverse photoemission spectroscopy is a custom made setup and is featured in chamber 1 of Figure 10. Photoemission spectroscopy is conducted in the analysis chamber (chamber 3) with a commercial setup from SPECS Surface Nano Analysis GmbH, Berlin, Germany. The excitation source for XPS is a magnesium anode being struck by an electron beam. This provides radiation at a fixed photon energy of 1253.6 eV. The source for UPS measurements is a helium discharge lamp providing a photon energy of 21.21 eV.

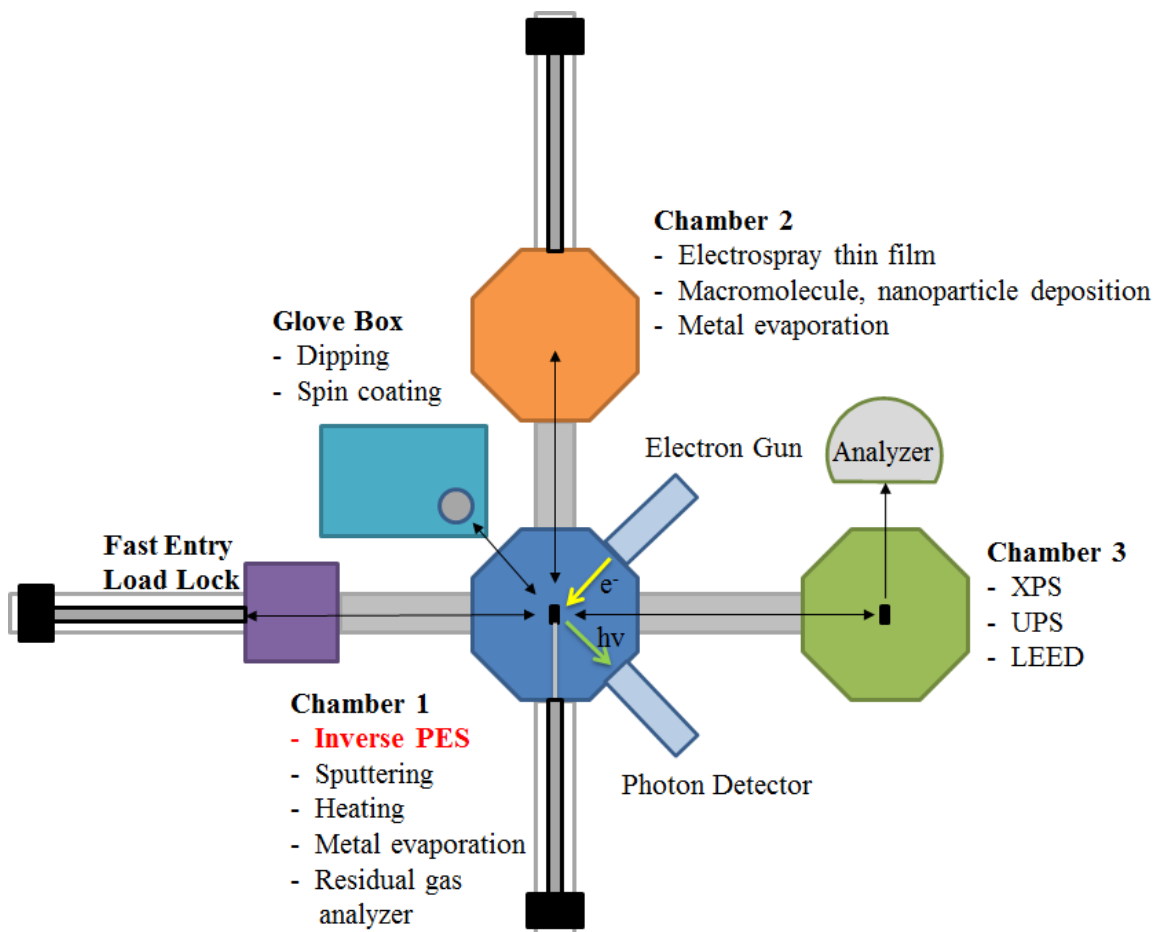


Figure 10: Integrated surface science system.

2.1.2 Sample Preparation

The samples analyzed were cut to size and mounted onto a substrate holder with dimensions 12.5 mm x 15 mm. For samples with a nonconductive back the screw heads provide an electrical contact to the sample holder and ground. The samples were cleaned with organic solvents (acetone, methanol and isopropanol). The polycrystalline Au was also cleaned by Ar^+ bombardment (SPECS IQE 11/35 ion source) for 40 minutes at a

kinetic energy of 5 keV and an emission current of 10 mA. This cleans the substrate surface from residual oxide and hydrocarbon contamination.

2.2 IPES Instrumentation

2.2.1 Electron Gun and Power Supply

The electron gun and power supply used in IPES is the ELG-2/EGPS-1022 electron gun and power supply combination supplied from Kimball Physics. The power supply is shown in Figure 11. This electron gun features both low and high energy modes combining for a range of 1 eV to 2000 eV. The beam current can be varied from 1 nA to 10 μ A depending on the applied grid voltage. The cathode is a Tantalum disc that is heated to approximately 2000° K to generate a stream of electrons through thermionic emission. The electron gun can be controlled via the Flex Panel display on the power supply or the Kimball Physics LabVIEW program [32].



Figure 11: Kimball Physics EGPS-1022 power supply.

2.2.2 Photon Detector

The photon detector in the system was custom built. The cathode tube, made by Torr Scientific, has a window at one end made of CaF_2 and a $2\frac{3}{4}$ " CF flange on the other. The optical low pass window filter is approximately 1.5 mm thick. Length of the tube is 11.81" and its outer and inner diameters are 0.87" and 0.71", respectively. The anode, shown in Figure 12, is a polished stainless steel electrode with a diameter of 0.12" which narrows to 0.06" near the tip.

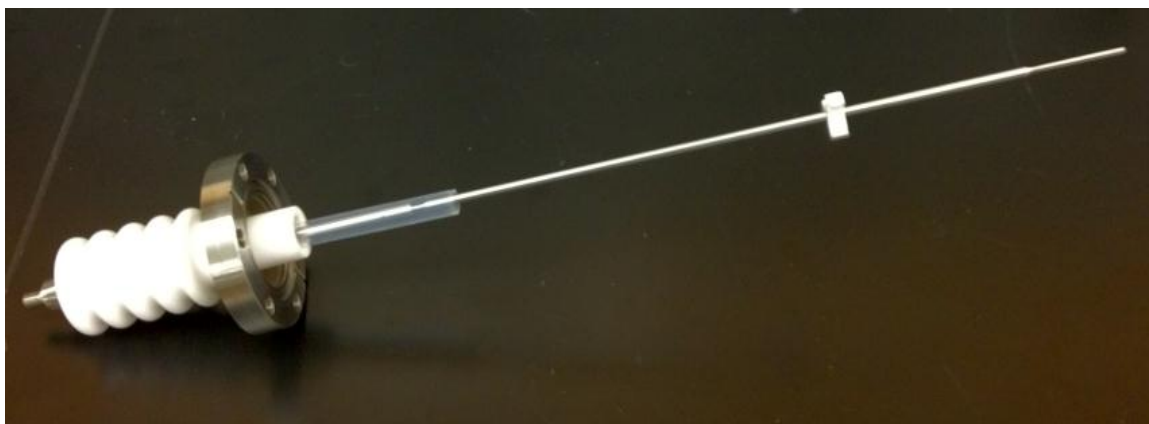


Figure 12: Electrical feedthrough and anode.

The electrical feedthrough was custom built by MPF Products, Inc. It is a high voltage feedthrough with a ceramic insulator rated up to 30 kV to ensure no arcing occurs inside the tube when the gas mixture is present. The electrical feedthrough was custom designed to be of the same material as the anode and with the same outer diameter. This allows for a good contact via the custom made sleeve that connects both electrodes. There are tap holes in the sleeve which prevent the trapping and later outgassing of

unwanted gasses. A Teflon cover extends over the sleeve to avoid arcing between the thicker diameter sleeve and the cathode. A Macor part cut to the inner diameter of the tube is placed approximately 2/3 of the way down the electrode to stabilize the tip and ensure centered orientation within the cathode. Figure 13 shows the assembled electrical feedthrough and detector.

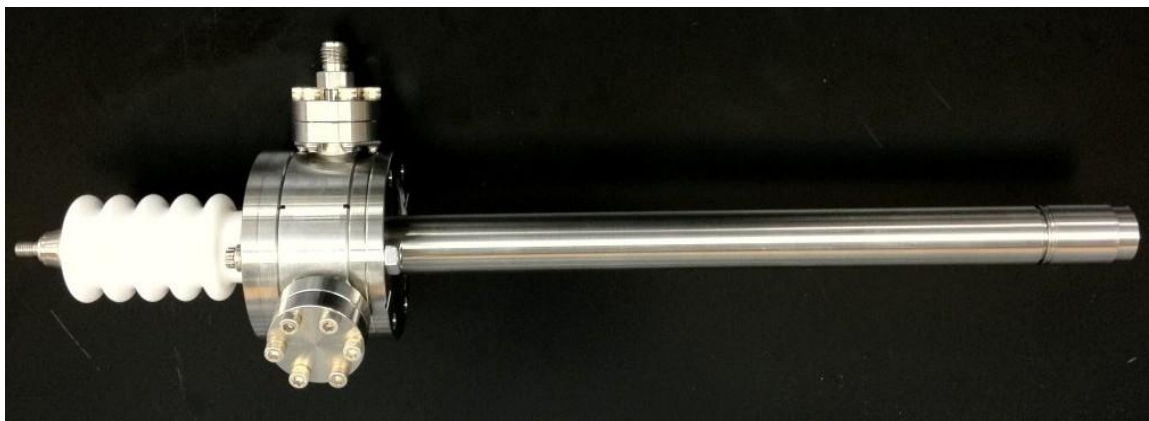


Figure 13: Feedthrough connected to CaF₂ viewport.

2.2.3 Gas Manifold

The gas manifold allows filling up the photon detector through a series of valves. Figure 14 shows a schematic of this manifold. Argon with a purity over 99.9% and complementary metal-oxide-semiconductor (CMOS) grade acetone with a minimum purity of 99.5% are used in the system. The manifold, and by extension the photon detector, can be pumped down via the turbomolecular vacuum pump as seen in the top left of Figure 14.

A Thermovac TR 211 (Pirani) gauge is used to measure both the acetone and argon pressures when filling the photon detector. The TR 211 gauge has an aluminum sensing cell with a tungsten filament and a measurement range of 5×10^{-4} to 1000 mbar. The filament is part of a Wheatstone bridge and when the temperature of the filament changes due to pressure then the control circuit will change the applied power accordingly to reach the nominal temperature and balance out the Wheatstone bridge. The gauge comes fully aligned and compensated for temperatures 0 to 40 °C. Paired with the gauge is a Combivac CM 31 controller to make the necessary power changes and calculate the pressure for the type of gas being measured. The calibration factor used for the acetone is N2 while the argon reading uses the Ar calibration factor.

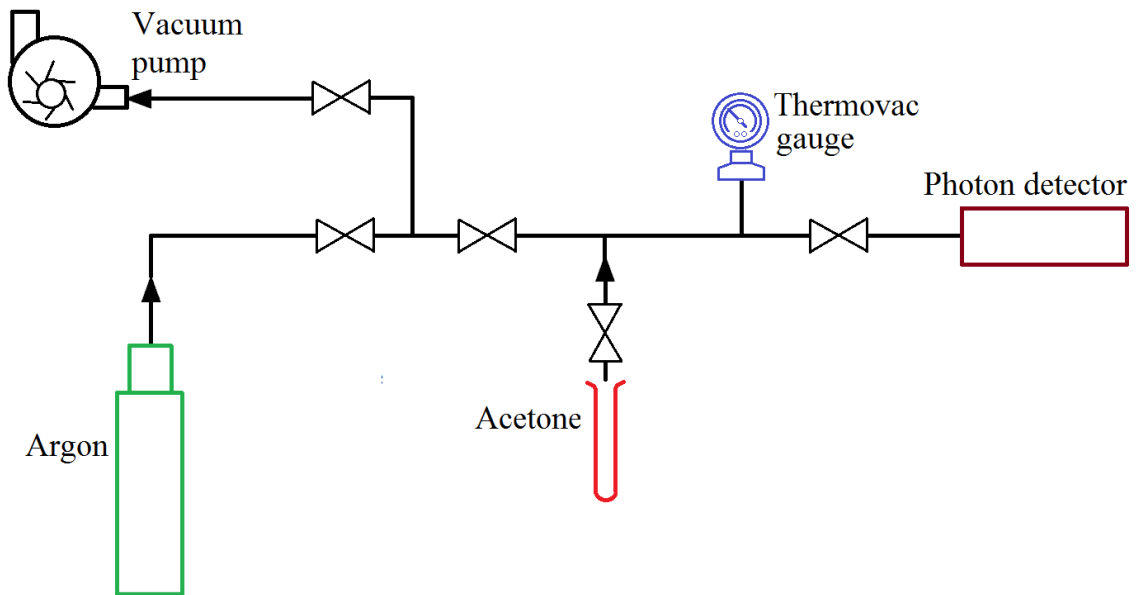


Figure 14: Gas manifold system for pumping and filling detector.

2.2.4 Counter Electronics

The electronics used to interpret the detected current pulses consist of a Tennelec TC 175 preamplifier, Ortec 452 amplifier, Canberra 2030 single channel analyzer, Ortec 4001A NIM BIN and a National Instruments PCI-6025E Data Acquisition (DAQ) card.

The Tennelec preamplifier is a charge sensitive preamplifier specifically designed to be used with proportional counters requiring up to 5 kV of bias voltage. It offers a sensitivity of 200 mV/pC and the input field effect transistor (FET) is protected against drastic changes in the bias voltage. The preamplifier routes the high voltage bias through the instrumentation box and outputs to the photon detector. The current pulses are then sensed and converted to voltage pulses. A test input is also available which is utilized later in Chapter 4 for the testing of the counter electronics.

The Ortec 452 amplifier has a variable gain from X2.5 to X3000 and a selectable shaping time constant of 0.25 μ s to 6.0 μ s. Changing the output range and the polarity can also be accomplished through the front panel. Other features not used in IPES include base line restoration and time delay insertion. The amplifier is connected to the NIM BIN power supply and has an output for the preamplifier power as well.

The amplified signal is then fed into the single channel analyzer (SCA). The SCA analyzes the peak amplitude of the incoming pulses and outputs a digital high/low (5 V/0 V) accordingly. This logic output is determined by the lower level and window settings on the front panel. The lower level can be adjusted between +.01 VDC to + 10.00 VDC and is used to set the lower discriminatory level to filter out noise in the system. The window can therefore be set to any value between the lower level and + 10.00 VDC.

The NIM BIN power supply is used to power all the counter electronics. It includes wiring for ± 6 V, ± 12 V and ± 24 V. There is a wiring harness delivering the power to the module connectors.

The output of the single channel analyzer is fed into the NI SCB-100 shielded I/O connector block for interfacing to the peripheral component interconnect (PCI) card. The National Instruments DAQ card receives the high/low signal from the connector block and inputs to the PC for acquisition and plotting. The PCI-6025E features two 12-bit analog outputs, 32 digital I/O lines and two 24-bit counters. The PCI card interfaces with the computer via the NI-DAQmx driver software and can stream to the disk at rates up to 200 kS/s.

A picoammeter, Keithley 6485, was used to continuously record the sample current during IPES measurements. It can measure currents from 20 fA to 20 mA with a resolution of 10 fA. Up to 1000 readings per seconds can be obtained. This current is used by the designed LabVIEW software to normalize the time scanned so the count rate is a true indication of counts per set charge.

The Stanford PS-350 power supply is the high voltage source used to create an electric field between the anode and cathode and is responsible for the photon detector's region of operation. It can provide high voltage DC output up to 5000 volts and is controllable from the front panel but also features serial RS-232 support which is implemented in the IPES LabVIEW program for remote control.

2.3 LabVIEW Software

A LabVIEW program was written to analyze the data coming in from the DAQ card. This software is designed for engineers and scientists to develop measurement, test, and control systems through a graphical environment. The dataflow programming language is referred to as G.

The program designed for IPES allows for data analysis and logging as well as control of external components such as the Kimball Physics electron gun and the Stanford power supply. For ease of use the program has been divided into three different tabs: manual mode, automatic mode, and detector voltage scan mode.

2.3.1 Manual Mode

The manual mode shown in Figure 15 allows the user to measure the counts coming into the system for a specified electron beam energy emitted from the gun. This beam energy is controlled by the Kimball Physics software while in the manual mode. A shared feature between all the modes is the ability to control the high voltage power supply to the photon detector via the software. This power supply control has its own box for turning on/off the power supply as well as setting the voltage desired followed by the output voltage reading from the supply. Within manual mode there are two ways to scan for the count rate. Counting mode allows the user to set a number of counts and the software will measure the time it takes to reach those counts. The alternative is timing

mode where the time is set and the counts are measured within this time. Both methods also allow having the scanned data be outputted for saving in a file.



Figure 15: Manual mode for IPES measurement at a fixed electron energy.

2.3.2 Automatic Mode

The second tab in the LabVIEW program is automatic mode. The first mode is used to measure the count rate at a specific beam energy while the automatic mode is used to scan the sample in isochromat mode where the detected photon energy is fixed and the incident beam energy is varied. There are various parameters that can be set to control the electron beam such as start and stop energies, step in eV, charge in μA , and number of scans to perform. These values are shown on the left-hand of Figure 16. The start and stop energies determine the beam energy coming out of the electron gun. The step size sets the resolution of the scan. This software resolution can be any value but is limited in practical terms by the physical resolution of the beam energy and the photon detector. The charge in μAs will establish the time for the program to acquire pulses at each step. This mode also contains parameters that are saved to the output file along with the power supply controls found in the other tabs. The saved parameters include acetone pressure, argon pressure, counter voltage, and the Fermi edge value that has been determined from a gold sample. All parameters are saved along with the control values to the output file for documentation when analyzing. There are two graphs which show the current scan and the average of all scans at any given time.

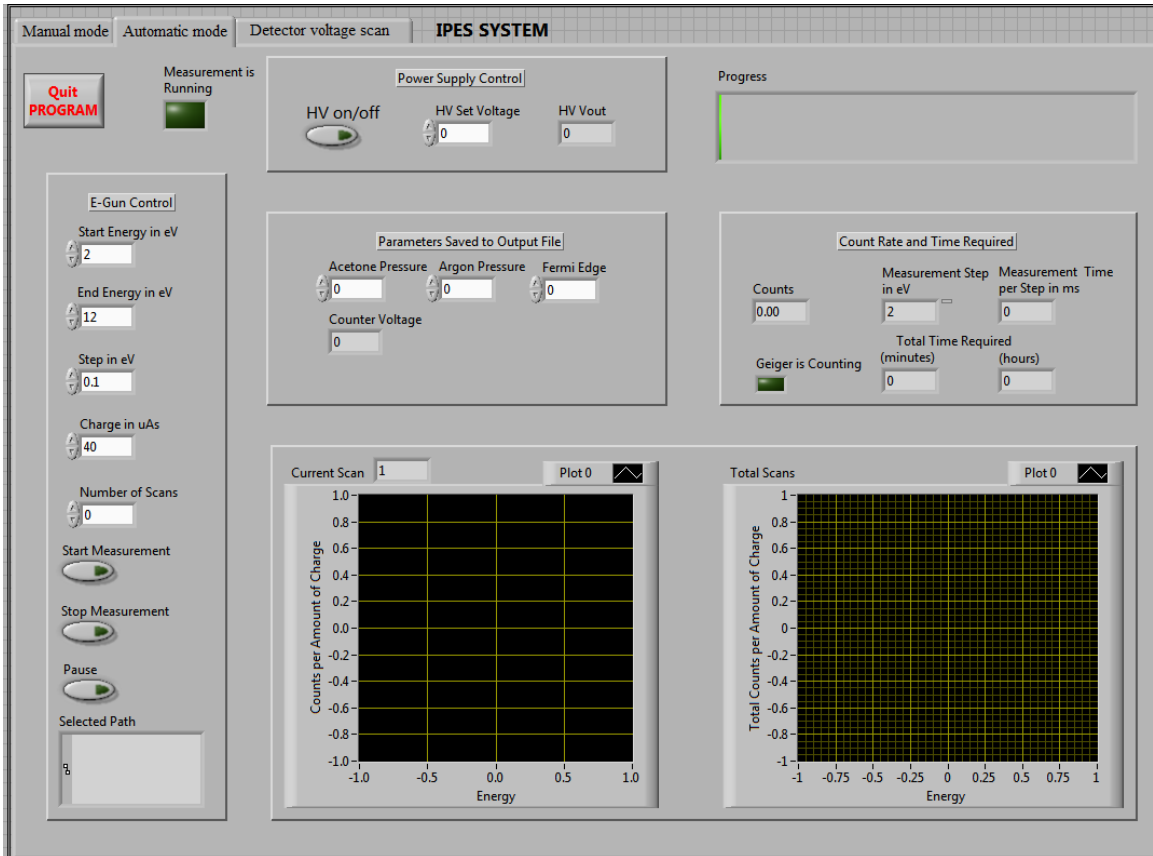


Figure 16: Automatic mode for scanning a spectrum of unoccupied states in a material by varying incident electron energy.

2.3.3 Detector Voltage Scan

Detector voltage scan mode is shown in Figure 17 is used when trying to determine what high voltage is required for photon detection after filling the detector with gas. If the applied voltage between anode and cathode is too low then ion-pair creation cannot be detected as the electric field will not be enough to accelerate electrons towards the anode. Inversely if the applied voltage is too high then the counter will be unstable and counts measured are not necessarily due to ion-pair creation from incoming photons. Therefore the applied voltage is important for having a stable counter. There are

CHAPTER 3: PHOTON DETECTOR OPERATION AND TESTING

3.1 Proportional Counter Gas and Window Selection

The selection of the window material and ionization gas will determine the optical resolution of the system. The most commonly used window in recent publications is CaF_2 [33, 34]. Shown in Table 1 are some of the materials used as the low pass cutoff. Due to the low cross section of IPES the combination of window/gas has to be chosen for adequate counts and resolution. A too narrow resolution reduces the counts to unpractical levels. CaF_2 was chosen as the window material in the photon detector.

Table 1: Window element cutoff energy comparison.

Window	Cutoff Energy	Reference
BaF_2	9.3 eV	[35]
CaF_2	10.08 eV	[36]
MgF_2	10.97 eV	[22]

Traditionally, iodine (I_2) has been utilized to provide the high pass ionization threshold. Budke et al. [37] have analyzed the performance of a CaF_2 window used in conjunction with both iodine and acetone. With the CaF_2 /iodine combination the

resolution is approximately 700 meV (FWHM). Recent progress in IPES has led to acetone vapor used over iodine for a number of reasons. The greatest advantage to using acetone is a smaller energy resolution of about 400 meV. Iodine is also corrosive and can cause problems in the sealing surfaces with stainless steel. Lastly, acetone does not require dead time correction because it works in the proportional region [38].

Acetone has been chosen as the ionization gas of the system. The photoionization of acetone is plotted in Figure 18 and the cutoff is determined to be approximately 9.69 eV while the cutoff of iodine is 9.23 eV [39, 40]. Therefore, a smaller bandwidth results from using acetone instead of iodine.

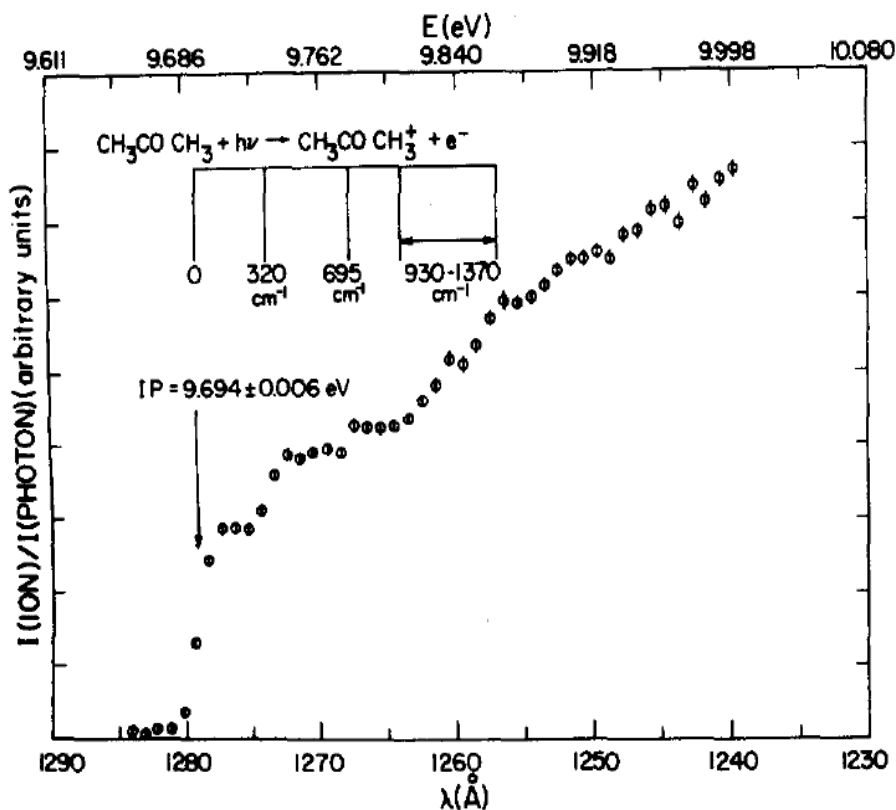


Figure 18: Acetone photoionization cutoff plot. Reprinted with permission from ([40]). Copyright 2012, American Institute of Physics.

The corresponding bandpass of mean photon energy $E = 9.9$ eV and an energy resolution of $\Delta E = 0.4$ eV has also been investigated by Funnemann and Herz [41]. Figure 19 gives a visual representation of the overlap between the two different filter elements. The blue line indicates the photoionization of acetone while the green line indicates the transmission curve of CaF_2 . The resolution is determined by the full width at half maximum (FWHM).

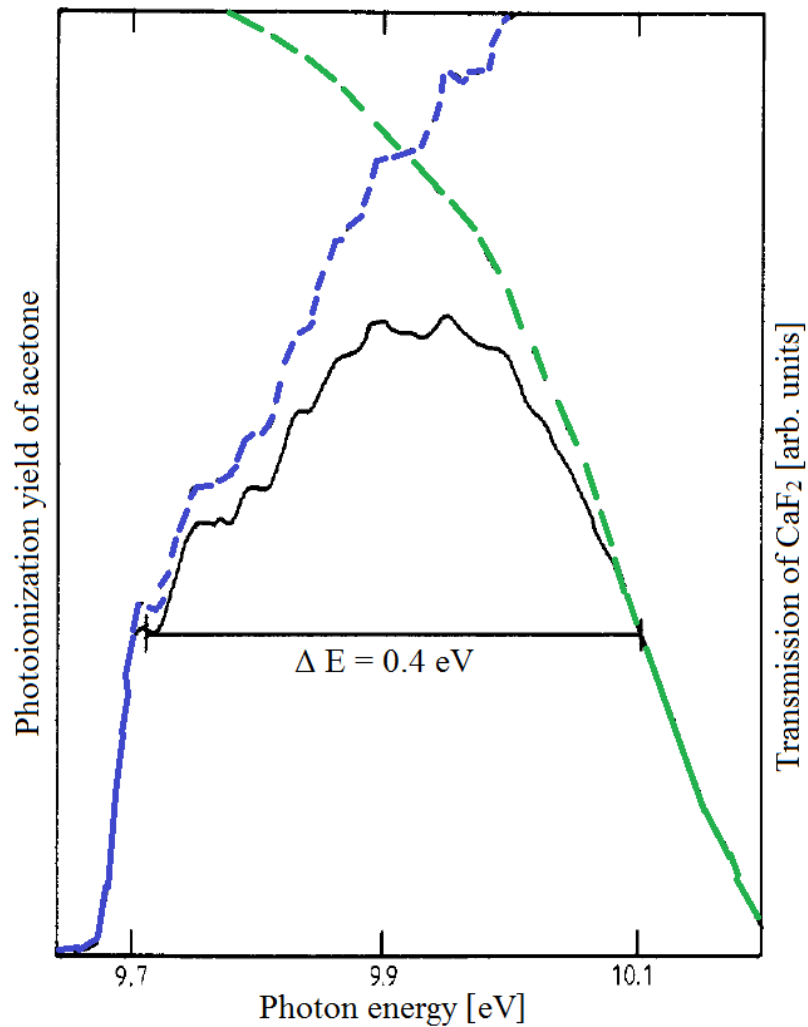


Figure 19: Overlap of acetone photoionization and CaF_2 transmission for the optical bandpass. [41]

3.2 Acetone Purification

The acetone was poured into a vial and then connected to the gas manifold system shown in Figure 14. While the acetone used in the vial is of high purity, there are gasses trapped in the remaining volume of the vial once it is connected. There are several ways of purification. Substitution of an inert gas by purging is one such method to replace reactive gases like oxygen and carbon dioxide. This method is not ideal since the desired final output is not the contamination free acetone desired. The freeze-pump-thaw method works by freezing the acetone and then evacuating the remaining volume to eliminate atmospheric gases. The latter method was deemed most suitable and implemented in purification of the acetone.

Initially the difficulty of freezing acetone arose from the low temperature required. The first thought was to use dry ice to freeze the acetone. The freezing point of acetone at 0 feet above sea level is approximately $-94.7\text{ }^{\circ}\text{C}$. At atmospheric pressure dry ice sublimates at $-78.5\text{ }^{\circ}\text{C}$ so it cannot lower the temperature of acetone to below its freezing point. Liquid nitrogen was therefore chosen as the cooling method to freeze the acetone. Liquid nitrogen boils at $-196\text{ }^{\circ}\text{C}$ so it can easily lower the acetone temperature to below freezing.

After the submerged acetone had frozen, the manifold lines were opened and the vial was evacuated for 2-3 minutes. Afterwards the liquid nitrogen submersing the acetone was removed and the acetone was left at room temperature to thaw. During the thaw cycle the acetone would exhibit gases rising to the top. This is the outgassing of other molecules into the now evacuated chamber above the liquid level. Once the

acetone had completely melted the cycle was repeated. For each subsequent freeze-thaw cycle the amount of outgassing dramatically decreased. After the third freeze-thaw cycle the acetone no longer outgassed and was then considered to be pure. Figure 20 shows the frozen acetone in the vial.



Figure 20: Frozen acetone while evacuating the vial.

3.3 Pressure Testing

The design of the photon detector and gas mixture is based on the previous work of Budke [37], Dose [26], Funnemann [41], Shukla [22] et al. After the assembly of the photon detector and the counter electronics, the gas and pressure mixture had to be determined. Both the gas mixtures provided by Shukla and Budke were tested.

The inverse spectrometer fabricated by Shukla et al. was published to work with only acetone in the detector. The gas pressure used by Shukla et al. was tested in the setup. A sputtered Au sample was loaded into the chamber via the fast entry load lock in Figure 10. The detector was then filled with only acetone to a pressure of 3.1 mbar (N₂ calibration). When trying to determine the count rate above the Fermi edge of Au as seen in Figure 5 of [22], the counts reached breakdown too quickly and no scan could be recorded. According to the literature the counts should first appear around 400 V with a peak around 620 V when the detector becomes unstable thus lowering the count rate. Different acetone pressures were tested and no stable operation was recorded. Table 2 shows the applied high voltage between the cathode and anode in the photon detector. The electron energy value on the gun was fixed above the Fermi edge to ensure a count rate could be perceived. The voltage was slowly ramped up from 0 V. Note there is no gradual increase in the count rate and no stable voltage where the measurement could be taken. The acetone gas mixture behaves too erratically. This is due to the fact that in the current setup without the multiplier gas it is almost impossible to detect the small current pulses on the anode. These small pulses can easily be hidden by the noise of the system. Counts only appear when the applied voltage is near the maximum recorded in literature. This is a very small window before the gas achieves breakdown and is no longer stable.

The acetone only gas did not prove to be successful so different mixtures were tested and will be subsequently discussed.

Table 2: The count rate vs. applied voltage for 3.1 mbar (N₂) acetone pressure is shown.

Applied voltage	Count rate above Fermi edge
<590	0
600	13
610	13
620	17
630	33
635	46
640	28
645	38
650	33
655	5001

The acetone and argon mixture tests are based on the operation of the spectrometer designed by Budke et al. The pressure used in that setup is a 1 mbar partial pressure of acetone with a total pressure of 200 mbar of the acetone and argon [37]. This was a starting point for the gas mixtures tested in this setup. It was decided that the use of a multiplier gas such as argon is essential to this configuration and should work well with the 1/200 mbar mixture.

The chamber was loaded with a sputtered Au sample again and then tested with different pressures. Once argon was added there was an instant change in the spectrum and the photon detector started measuring expected counts. The energy of the electron gun was fixed above the Fermi edge as it had been in the previous acetone only test. Around 500 V the first counts appear. The peak number of counts is around 525 V. The detector is functioning as it should. The plot in Figure 21 bears resemblance to the count rate scans for different pressures in Figure 5 by Shukla et al. [22]. It is of value to note that although the acetone only gas did not work as intended in this setup, the addition of the multiplier gas allows the counts to be identified and the plot now resembles similar data published by Shukla et al. [22].

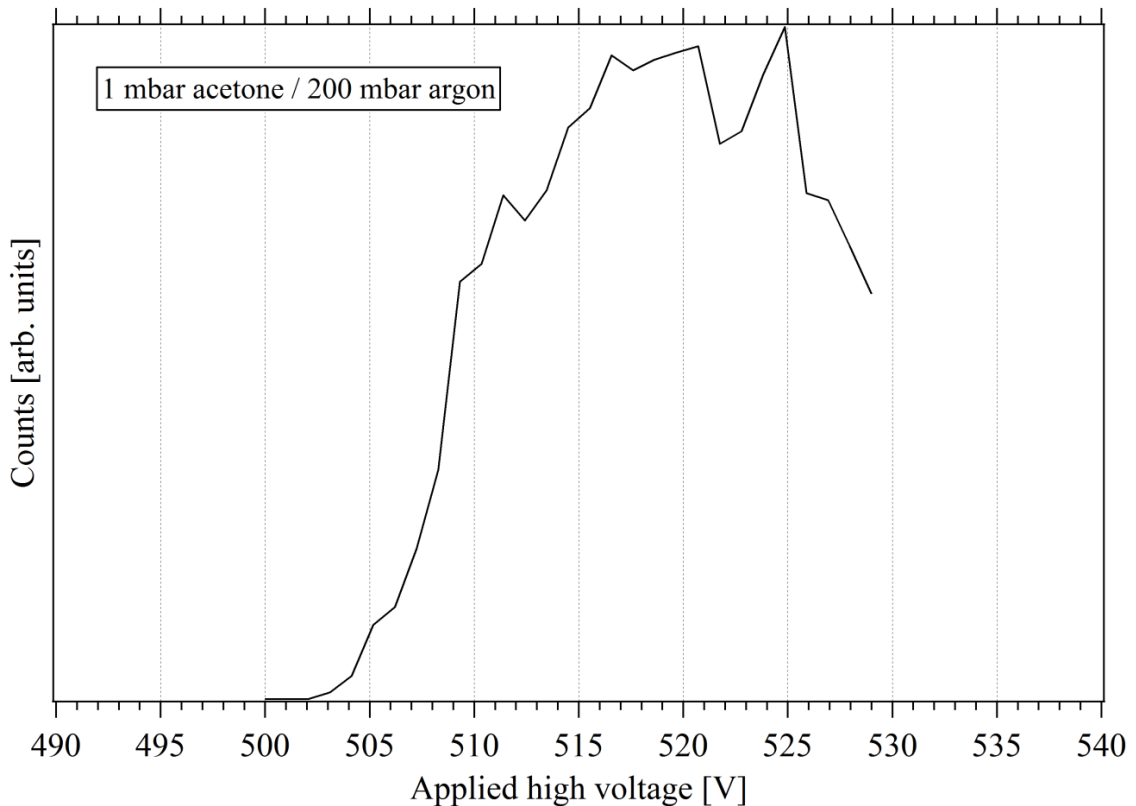


Figure 21: Count rate vs. applied high voltage for a fixed energy above the Fermi edge (1 mbar acetone / 200 mbar acetone and argon gas mixture).

The next step was to test other gas mixtures and see if this result could be improved. The acetone pressure was first kept constant and the argon pressure was varied. It is the argon pressure which amplifies the initial ion pair creation and makes the current pulse a detectable level so changes in amplitude will more likely be related to an argon variation than an acetone variation.

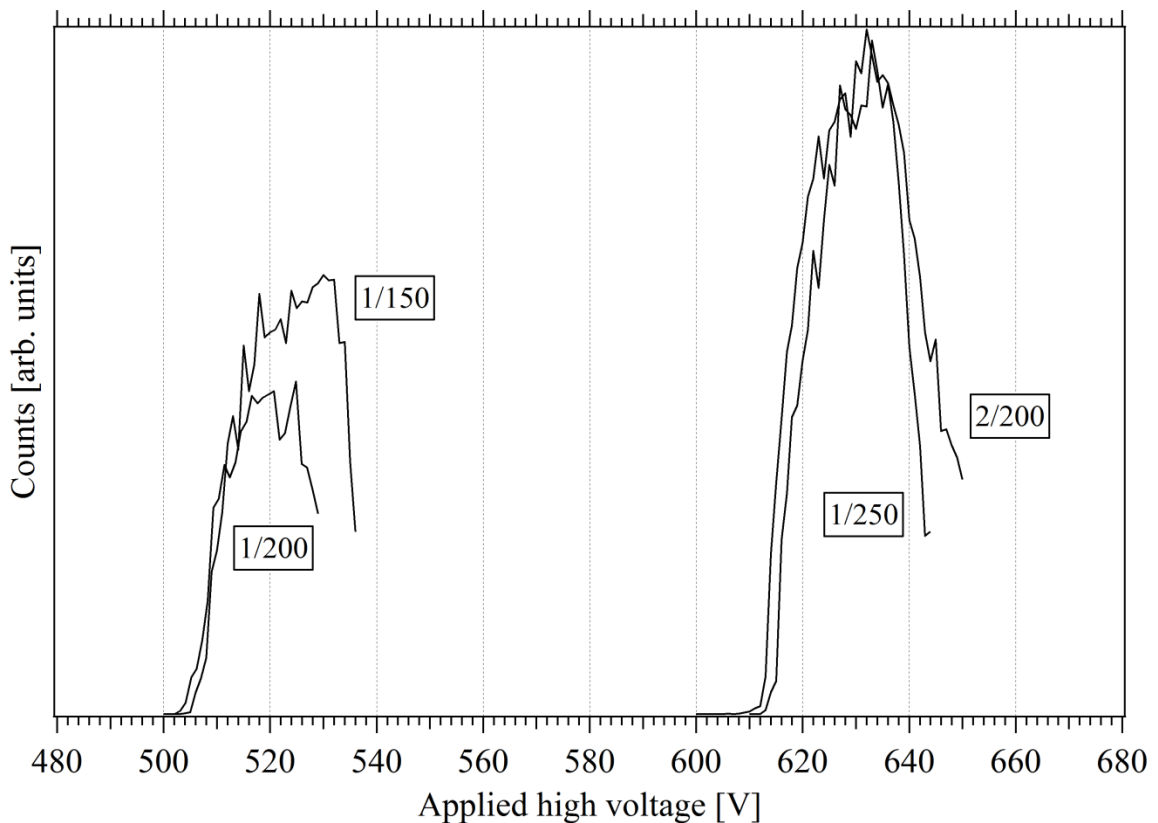


Figure 22: Count rate vs. applied high voltage for a fixed energy above the Fermi edge (varied gas mixtures).

The changes in count rate for different gas mixtures are shown in Figure 22. There are slight differences for the different mixtures such as higher count rate and a wider bandwidth of applied voltage. The plots do not differ substantially in way of

general shape and behavior. The onset of counts is shifted to a higher voltage for a higher concentration in acetone and in argon. The large separation can be accounted for by the pressure gauge used to measure the gas pressure in the photon detector. The thermovac gauge as discussed in the experimental chapter has a logarithmic pressure scale and when it reaches 200 mbar its step size has increased to 10 mbar. Therefore the resolution is larger when compared to pressure readings of lower magnitudes.

These scans help to determine the best mixture but it is in fact the consistent intensity of scans that would help identify the best mixture. The Au sample was then scanned at a fixed applied high voltage below the peaks of the scans shown in Figure 22. The energy range of the electron gun was varied from 2-14 eV. The Au sample was scanned 4 consecutive times. Lines in Figure 23 show the change in intensity of each scan. It is interesting to see that by decreasing the argon pressure in the detector each subsequent scan had the general trend of increasing. The reverse is seen when the argon pressure is increased. The mixture of 1 mbar acetone and 250 mbar shows this decreasing trend. In order to assume functional operation of the detector the results have to be repeatable with minimum deviation. The 2 mbar acetone and 200 mbar argon mixture also had sporadic deviation and is not suitable. The original mixture used by Budke was deemed to be a good operating mixture for this setup.

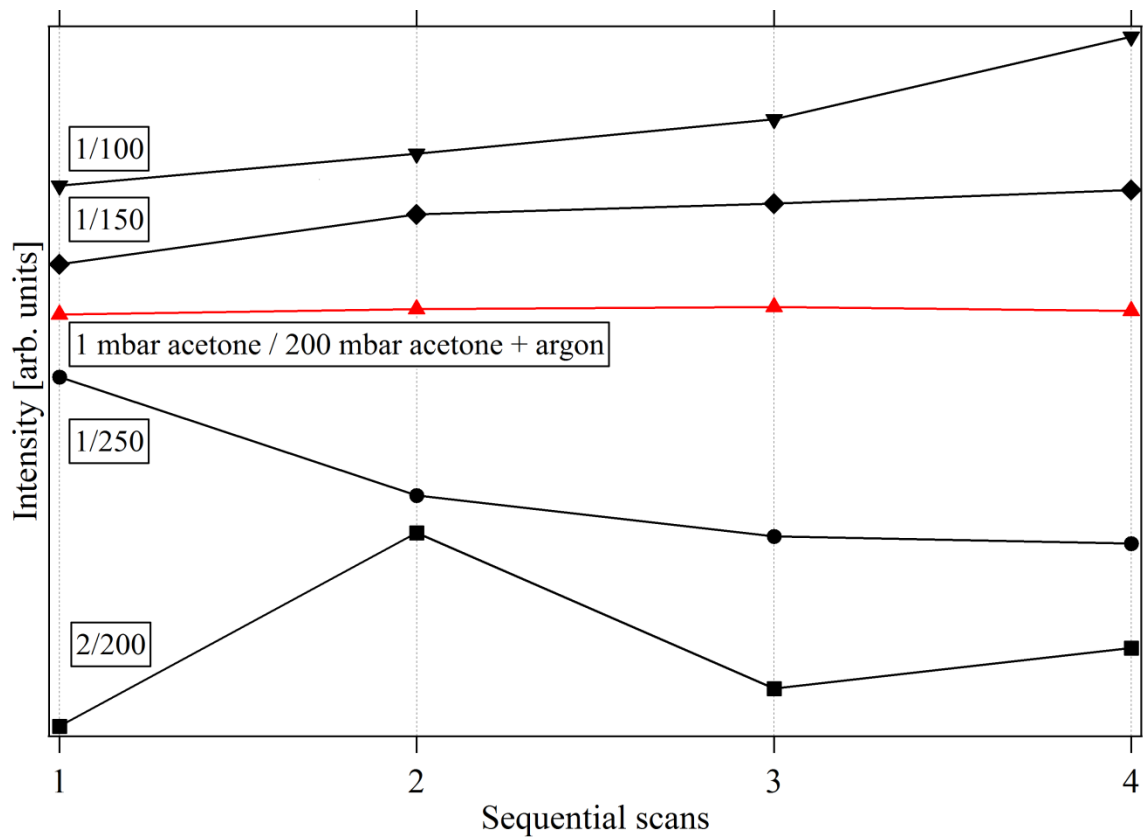


Figure 23: The various gas mixtures were used to scan Au from 2-14 eV and the intensity deviation has been plotted via the variation in each scan.

CHAPTER 4: SOFTWARE AND ELECTRONICS

4.1 Electronics Operation Test

The signal analysis electronics were tested in an isolated environment to ensure proper operation. Figure 24 through Figure 26 depict the signal input and output at each stage. A square wave was used as a test signal input to the preamplifier. This is shown as Channel 2 in the figures for reference.

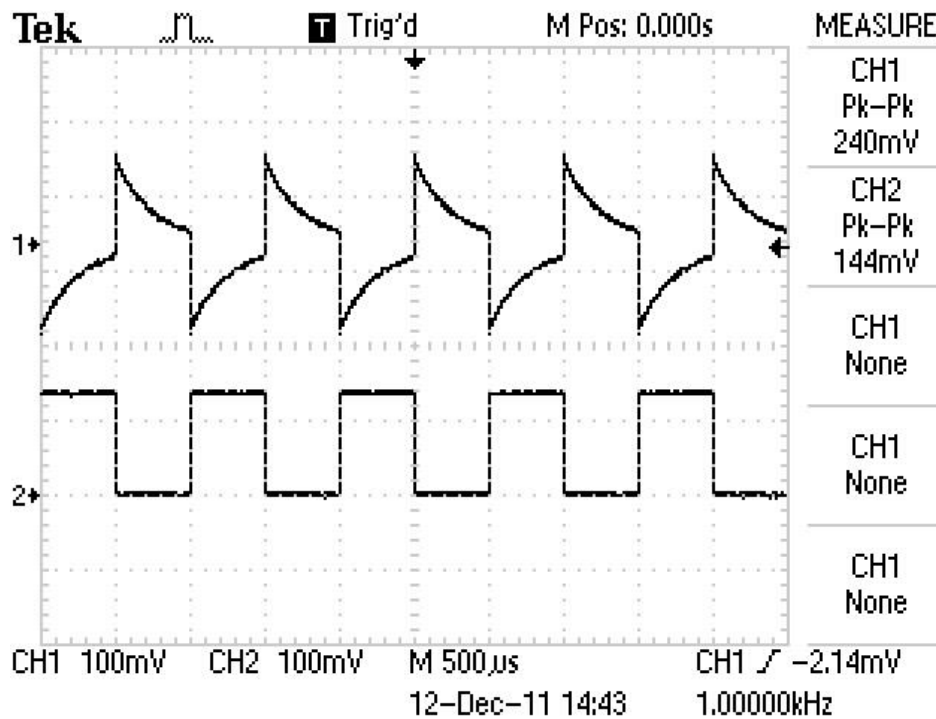


Figure 24: A square wave pulse is fed into the test input of the preamplifier (Channel 2). The output is the converted and amplified signal (Channel 1).

A characteristic of the preamplifier is that the output is inverted, as shown in Figure 24. This is nullified by inverting the output again at the amplifier stage so the proper rising edge outputs the positive pulse. The gain of the amplifier was set to X25 which is reflected in the signal amplitude change from 0.24 V to 6.32 V from transition of the preamplifer to the amplifier output. The pulse shaping characteristic is also shown in Figure 25. This setting is used to provide a more distinct pulse and is easier to isolate. Figure 26 displays the output of the single channel analyzer where a +5 V pulse is created for each initial current charge above the set noise threshold. It is this signal that is fed into the computer for further analysis.

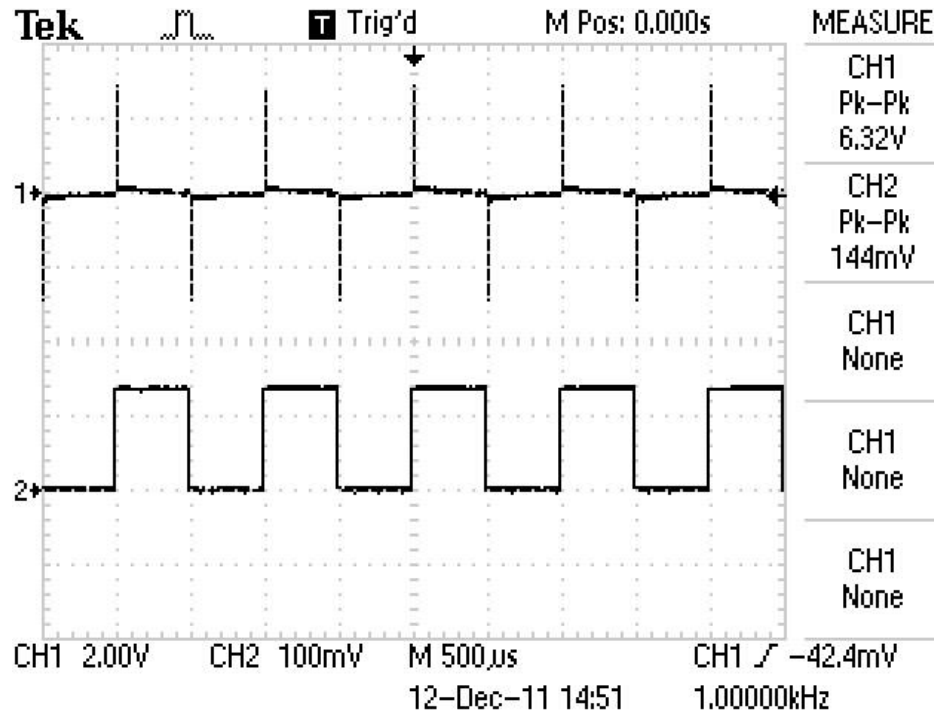


Figure 25: The output of the amplifier (Channel 1). The initial input to the preamplifier is shown as well (Channel 2).

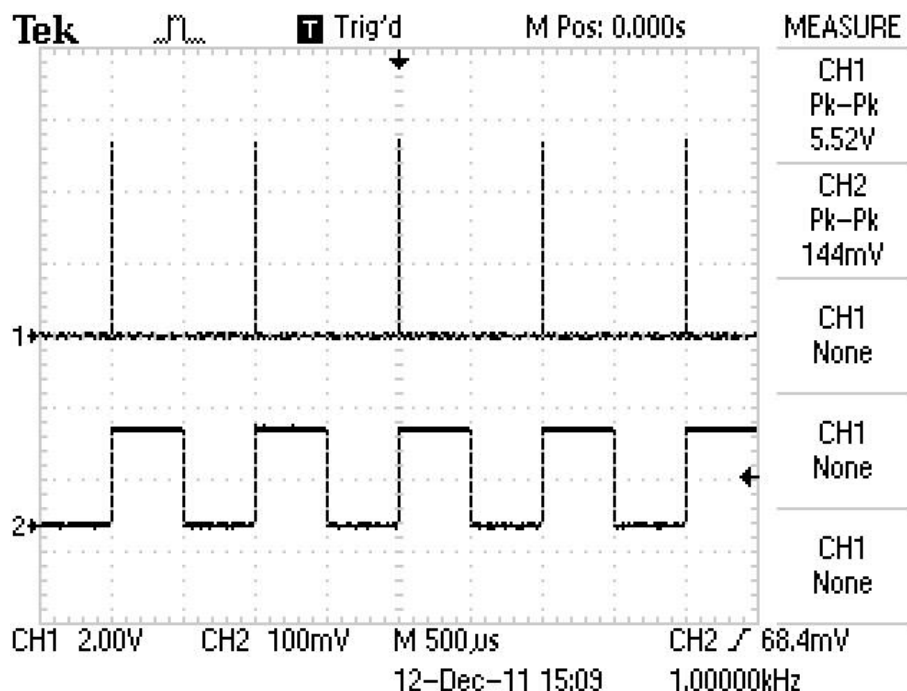


Figure 26: The 5 V output of the signal channel analyzer (Channel 1).

4.2 Electron Gun LabVIEW Interface

The electron gun and power supply mentioned in Section 2.2.1 are controlled by a LabVIEW program created by Kimball Physics. This fully functional standalone software controls most configurable aspects of the electron gun. There are many parameters that can be set as desired (e.g. beam energy, anode voltage and source voltage) but an important consideration is the possibility of damage due to drastic variations from the recommended operation of the gun and power supply. Kimball Physics has therefore put safeguards in place for several of the parameters. For example, the source voltage heating the cathode can only be increased by a maximum of 0.25 V at any time. Precautions ensure proper use of the gun and extension of the setup lifetime. The recommended startup and operation of the electron gun is featured in Appendix B.

In order to change the settings of the electron gun with the custom designed IPES software, it was necessary to have external access to the Kimball Physics software. The green rectangle by the electron energy in Figure 27 is a visual indicator that the parameter is being accessed by another virtual instrument (VI). This is achieved with data binding through DataSocket provided by National Instruments. This was specifically developed for the sharing of live data through a network over various protocols such as HTTP, FTP and local file access. In this program the data is accessed locally and is only necessary to allow the IPES software control over the electron energy from the electron gun. Therefore the energy control in the Kimball program was set to data binding into a local variable where only read access was allowed. Similarly the energy setting in the IPES software was set to have write access to the same variable. This is shown in Figure 28.

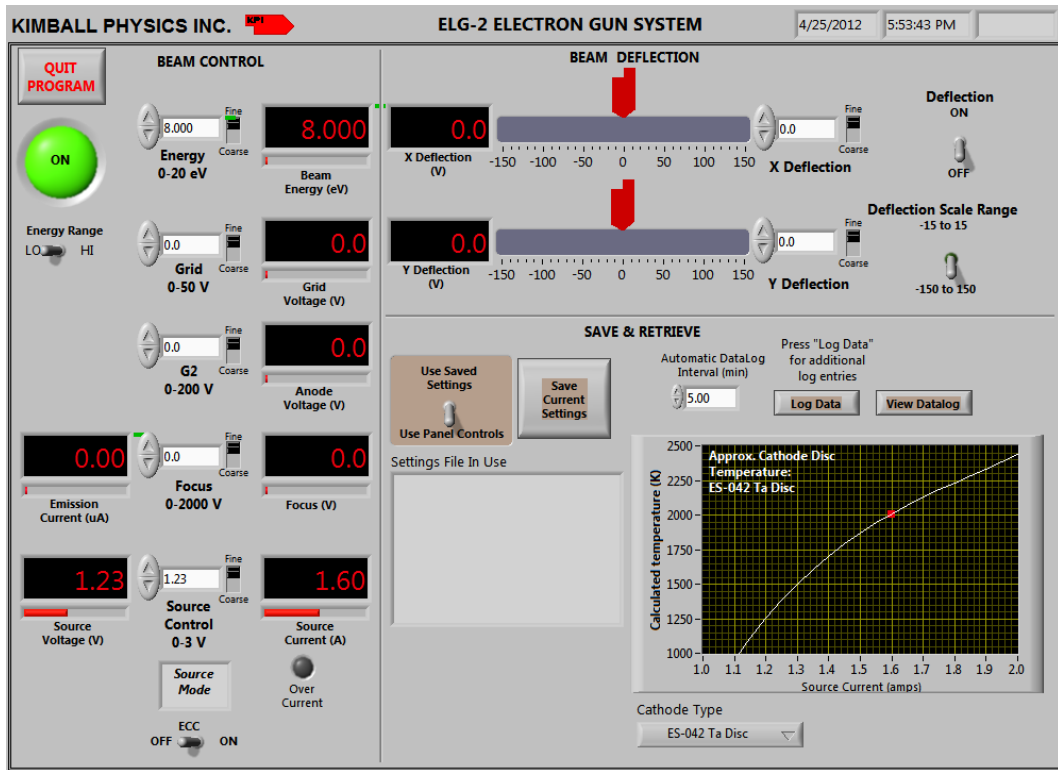


Figure 27: Electron gun LabVIEW interface created by Kimball Physics.

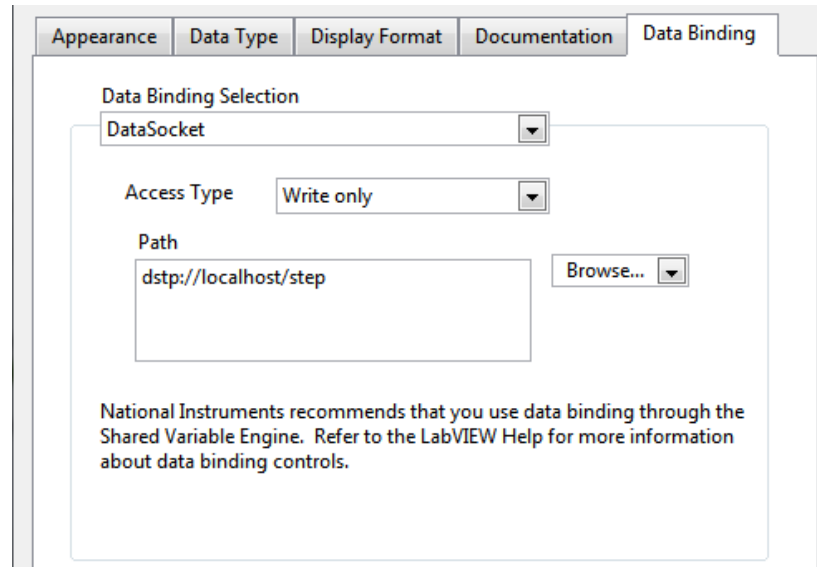


Figure 28: IPES software data binding to local "step" variable.

4.3 IPES LabVIEW Software

4.3.1 NI DAQmx

The count acquisition PCI-6025E card interfaces with the computer via the National Instruments DAQmx driver software. This is a new API design and architecture that was implemented in the 1990's to add several new features to the outdated DAQ software. The improvements include being able to add new devices with greater compatibility, taking advantage of newer CPU architecture and enabling multithreading. There are various performance gains and the new method of data acquisition has become simple. Perhaps the most important part of the IPES software is being able to distinguish the counts coming from the single channel analyzer. The DAQmx driver software makes this task very easy. The counting task shown in Figure 29 is accessed by the Measurement and Automation Explorer in LabVIEW. When the task is set to edge

counting, the device counts the rising or falling edges via single edge counting or buffered edge counting. For IPES counting the configuration is set to count the rising edges with the 1 sample on demand method. Once the counting is activated the task will start accumulating the counts until it is turned off.

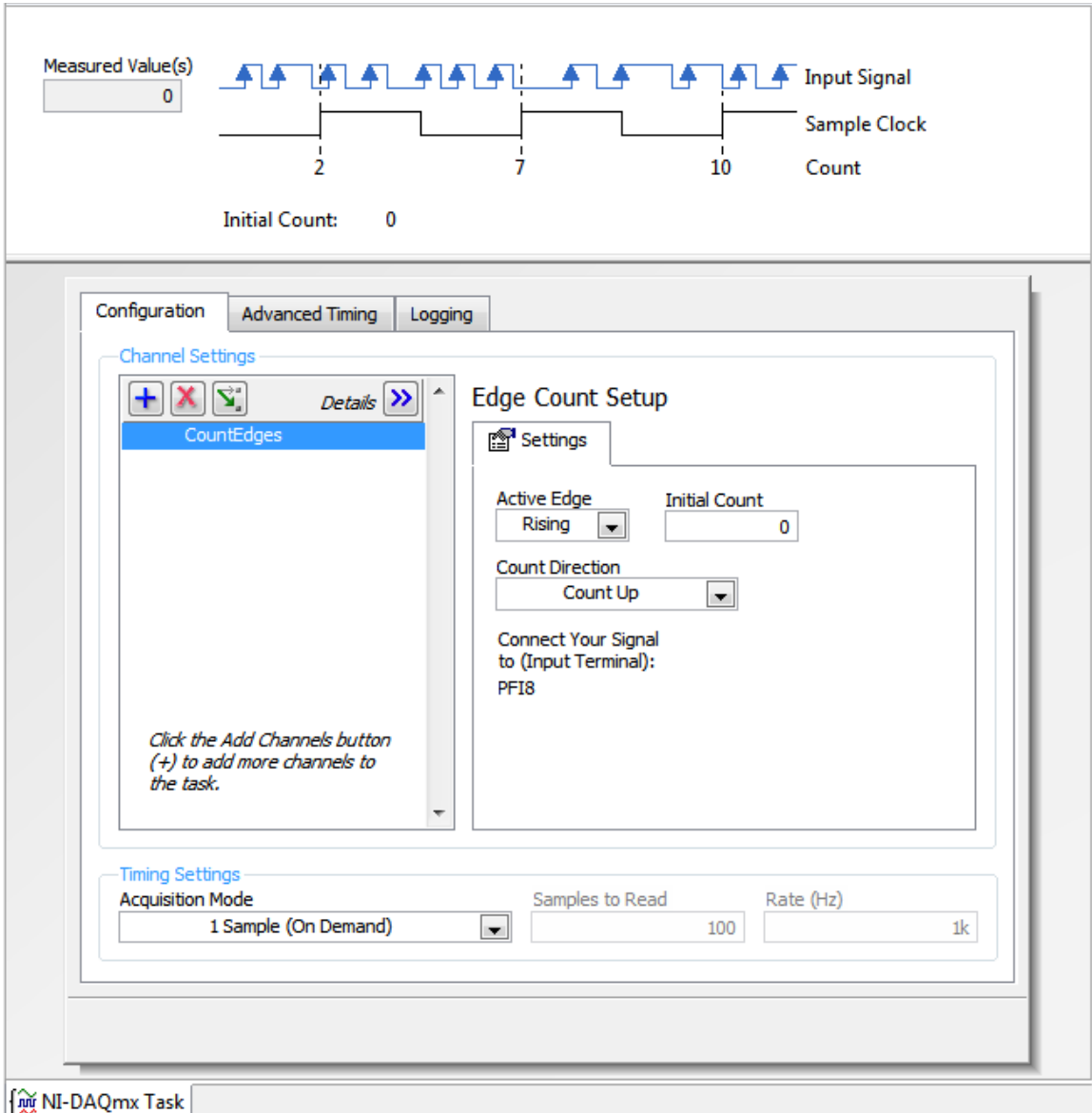


Figure 29: National Instruments DAQmx task to read counts.

4.3.2 Sample Current Reading

Initially the time required to scan at each step was determined from the measured beam current coming from the gun. When the accumulated current reached the set threshold, the software would stop counting and increase the beam energy by the step size to continue scanning.

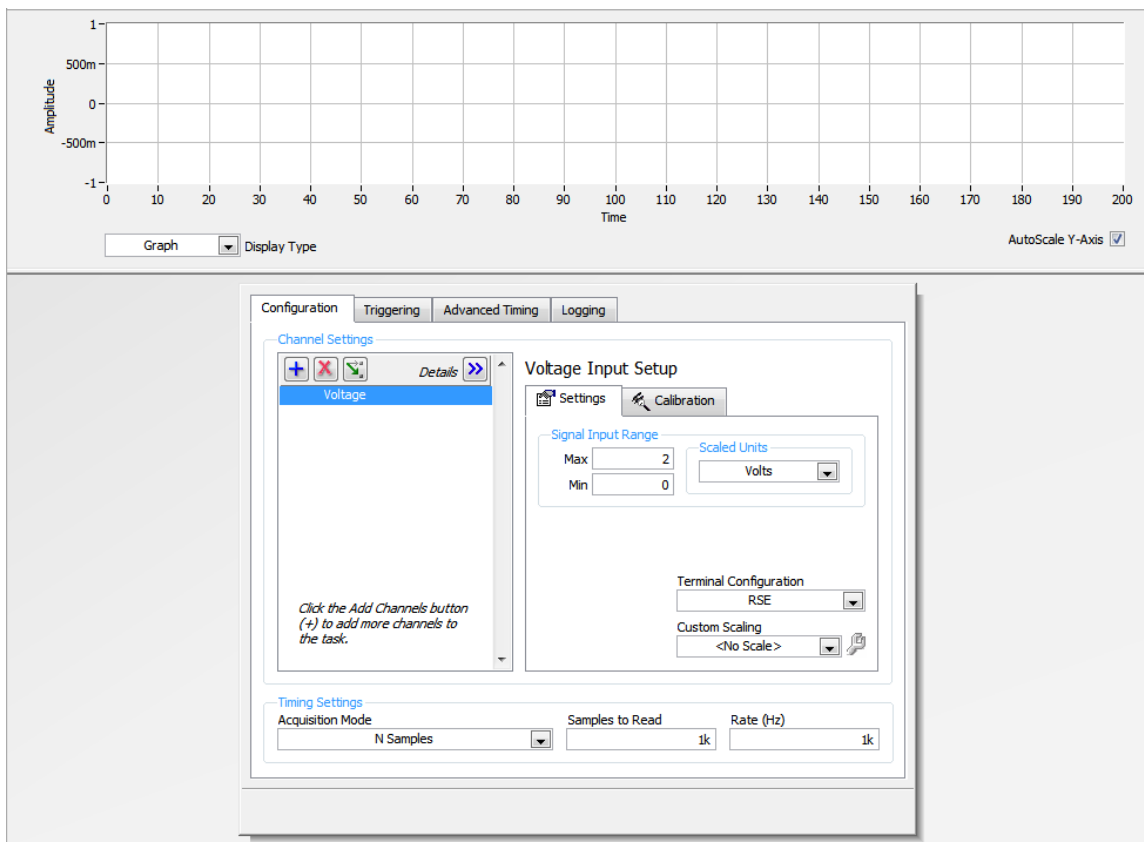


Figure 30: Sample current acquisition setup.

A picoammeter was then connected to the stage holding the sample to directly measure the sample current. This value is now used to define the time measured at each step therefore the count rate is a true indication of counts per set charge. The sample

current is needed to normalize the count measurement at each step due to variations of the current as the beam energy is changed. If the counts at each measurement are normalized to a set time instead, the change in current is not accounted for and the counts cannot be accurately compared. To implement this, the National Instruments data acquisition software was again utilized. Figure 30 shows the DAQ setup for the input. The picoammeter takes in a current value between 0-20 μA and outputs a mapped voltage from 0-2 V accordingly. The reading is taken at a rate of 1000 Hz. In the IPES software these values are averaged every 1 second to resolve the current reading that is taken for the step to determine time to count.

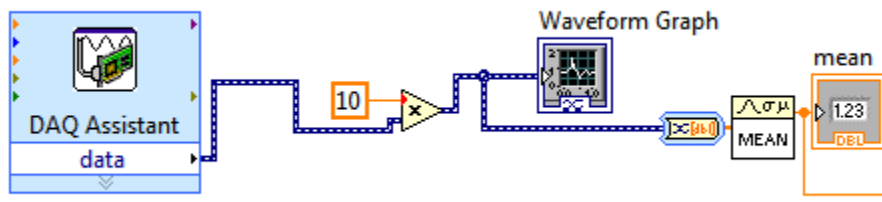


Figure 31: LabVIEW stage current reading and averaging.

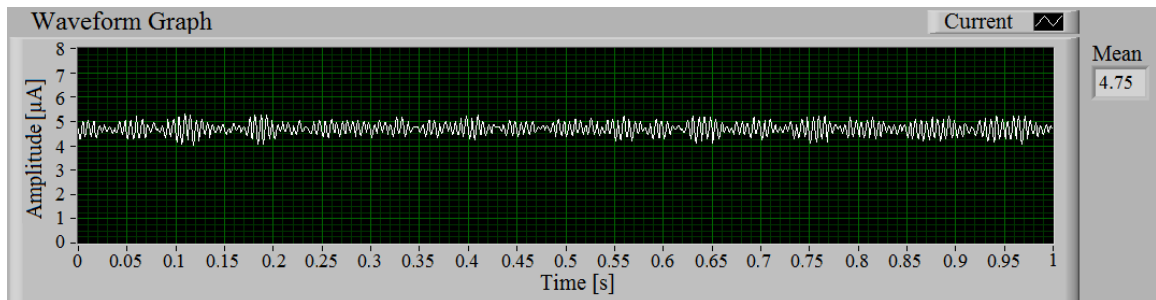


Figure 32: Sample current front VI display.

The plot of the sample current scan and the mean value is shown in Figure 32. The current is averaged over 1 second to take into account the slight variations shown in the graph. Note that the current values have already been converted to the proper 0-20 μA mapping in the back VI code for the sample current in Figure 31.

4.3.3 Stanford Power Supply Control

The IPES LabVIEW software has been designed to control as many aspects of the measurement as possible for easy operation. The control of the Stanford PS-350 high voltage power supply has been added to each mode in the program. Remote controlling of the power supply can be turned on and off and be set to any desired voltage. This value is verified by the output of the power supply on the VI. Figure 33 shows the control loop.

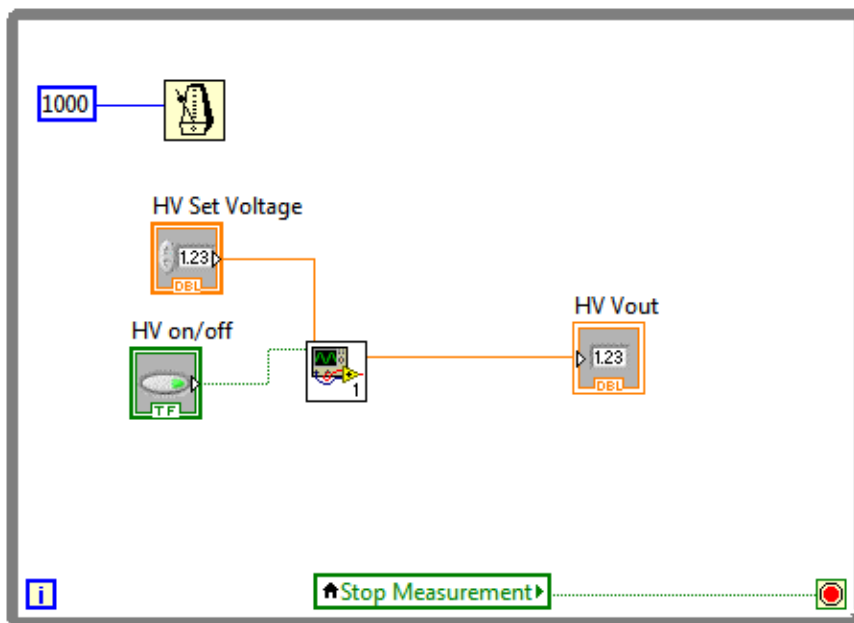


Figure 33: Stanford PS-350 LabVIEW control loop.

4.3.4 “Automatic Mode” Flowchart

The structure of the “Automatic Mode” of the software is shown in Figure 34 with a flowchart. This mode of the program encompasses a great deal of the functions featured in the other tabs, therefore it is discussed in detail. After starting the program the user has many parameters to input. Parameters such as the start and stop energies, step size, number of scans, and charge in μAs are required for each measurement. The remaining parameters which are enclosed in another structure in the graphical user interface (GUI) are not necessary but are important and will also later be saved in the data file.

After the parameters are set the scan can then be started. First the array and scan number are initialized. The acquisition of the driver software to register the counts follows. There are three loops in the automatic mode. Starting from the outside and working in, the first loop checks to see what number scan is currently being run and if the set number threshold has been reached. The second smaller loop is responsible for energy range adjustments of each scan. This loop will compare the current energy of the electron beam and determine if the maximum desired value has been reached. Lastly, the smallest loop is for the energy comparison at each different step size. This measures the sample current that has accumulated at a step and compares it to the preset current threshold value to ensure the counts are comparable. At the end of each scan an array is built with the scan data and the parameters first input to the GUI. This array is automatically saved in a text file labeled with the scan number. Once the final scan ends, another array is created and saved, which includes all of the averaged scan information.

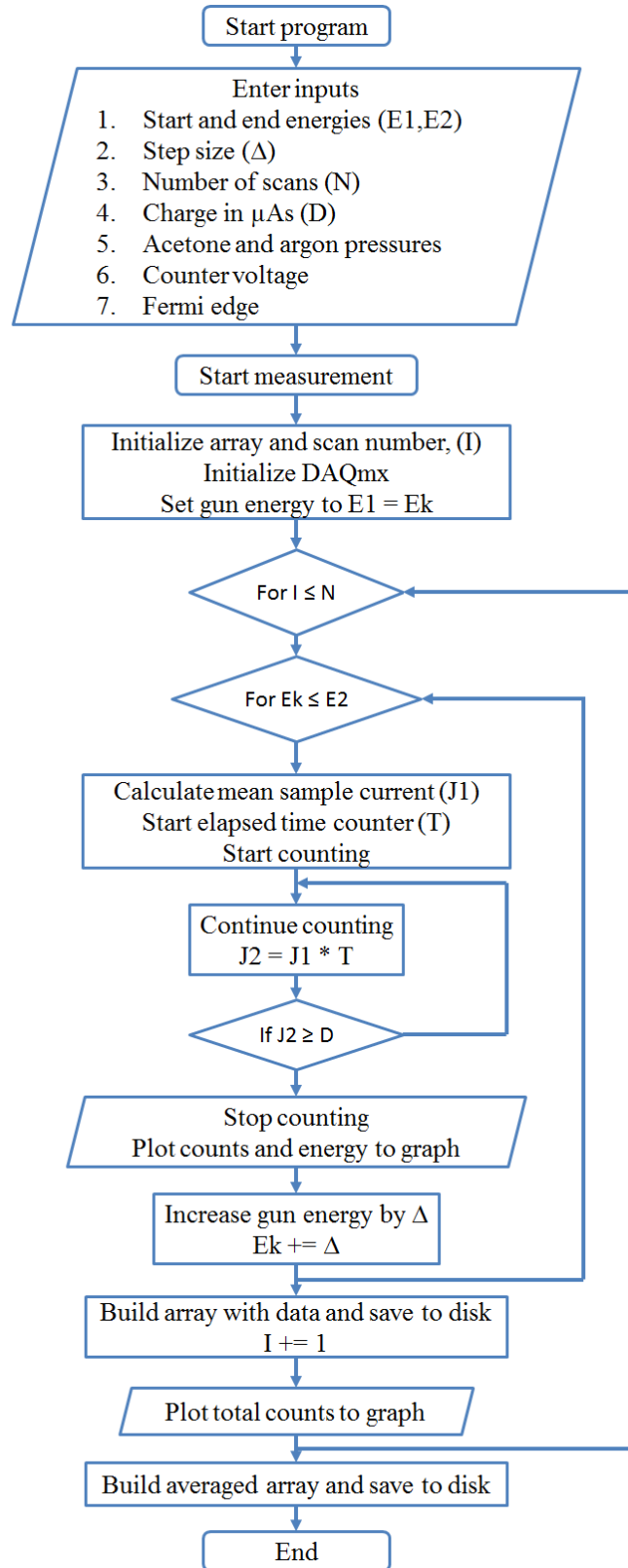


Figure 34: Automatic mode flowchart.

4.3.5 Data Acquisition

The basic overview of the program has been presented but a more thorough description of the code is required to show how each step is achieved.

The data acquisition is similar in all 3 modes, the most complex of these being the “Automatic Mode”. This mode is explained in detail in this section. The arrays are first initialized with all zeros shown in step 1 of Figure 35. The beam energy is one of the array inputs. It is at this stage where a desired Fermi edge shift can be taken into account. The Fermi edge is by default set at 0 eV but can be changed to a desired value once the Fermi edge of the system is determined. The other array input is the counts measured at each step. These two arrays are then combined and transposed for later manipulation. The two values are also used to build a graph which will show the user the current scan progress.

The count acquisition that is stored in the array of Figure 35 is shown in detail in Figure 36. The DAQmx driver software reads the counts from the previous setup where the PCI card is input the single channel analyzer signal. This is all contained in a while loop. The counts are detected and accumulate until the set charge in μAs is reached using the mean sample current. After the while loop is terminated, the total counts for that respective step are saved to the previous array.

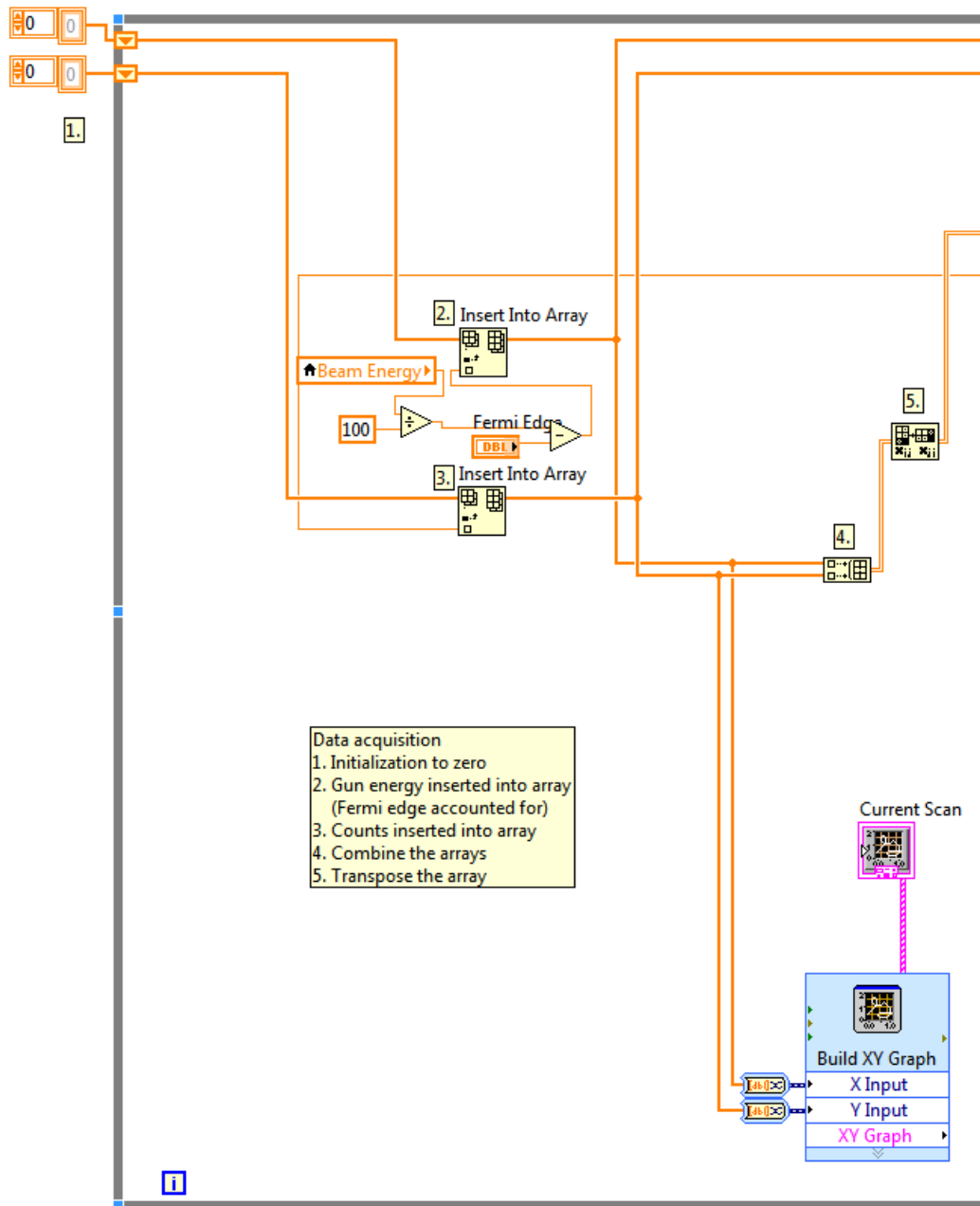


Figure 35: Count rate array creation.

The next data structure shown in Figure 37 is used to increase the electron energy according to the step size. The measurement energy is increased by the step size and thereafter checked against the set end energy of the scan. Because the energy readings

from the electron gun vary slightly and are not equal to integers, 0.01 was added to the end energy comparison to assure that the final step was not overlooked and the scan ends prematurely. The newly increased measurement energy is then fed into the “measurement step in eV” parameter which will write to the DataSocket and the electron energy will be increased. After the measurement increase there is a delay inserted to suspend counting while the electron gun adjusts to the new energy. If the end has been reached and the current energy is higher than the end energy, the gun energy is dropped back down to the initial value of 2 eV.

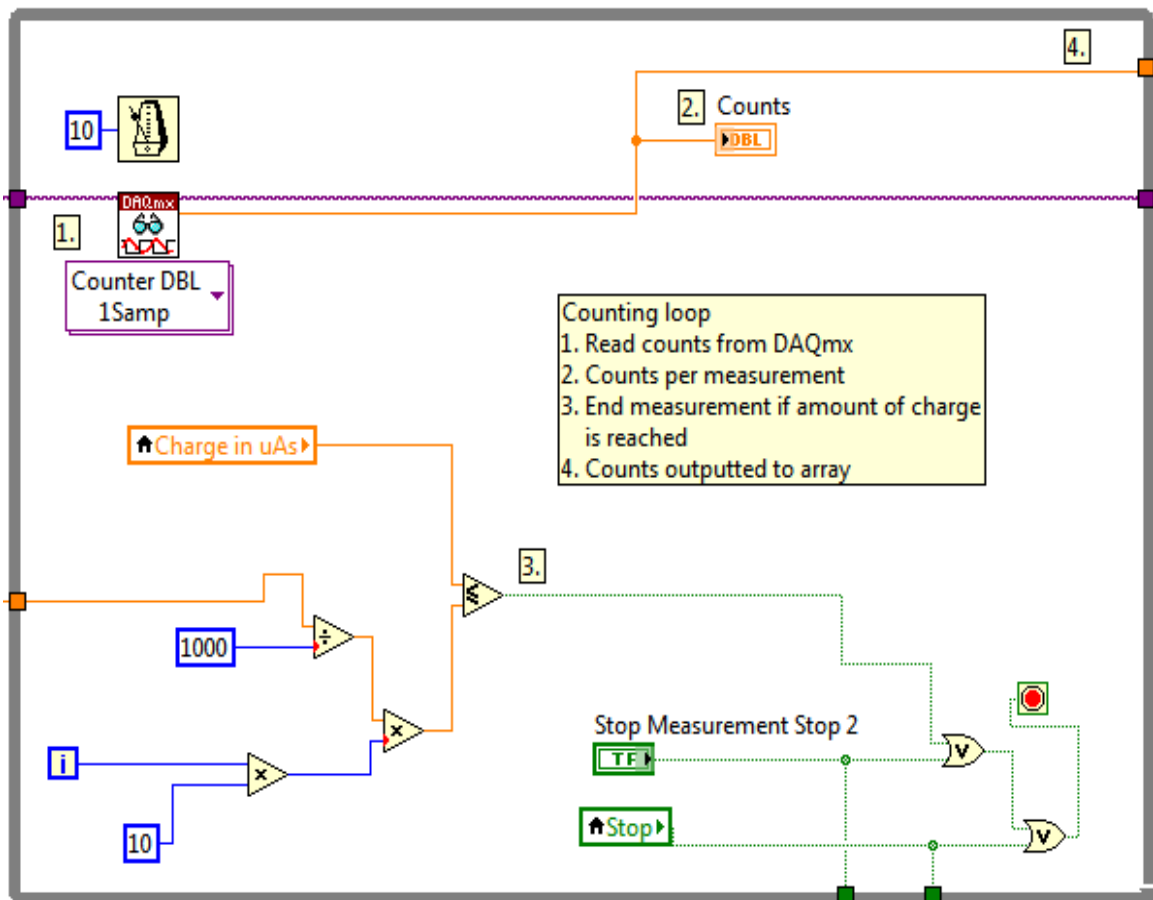


Figure 36: Counting loop for each individual step measurement.

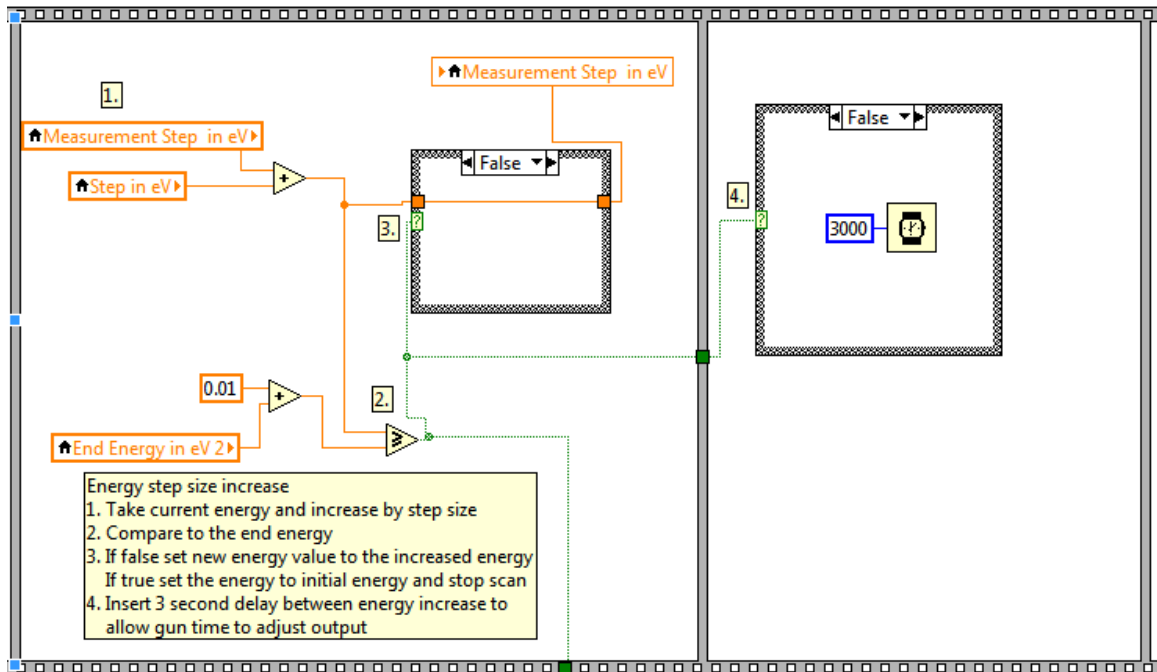


Figure 37: Energy step increase structure.

When the full range scan has completed the data has to be saved. The array has been building with every step measurement. Now this completed array is taken and certain information is added. In the initial setup before starting the scan several parameters were designated. These values are then stored along with the count information. The parameters include:

- Acetone and argon pressure
- Counter voltage
- Number of scans
- Charge in μAs
- Step in eV
- Fermi edge
- Start and stop energies

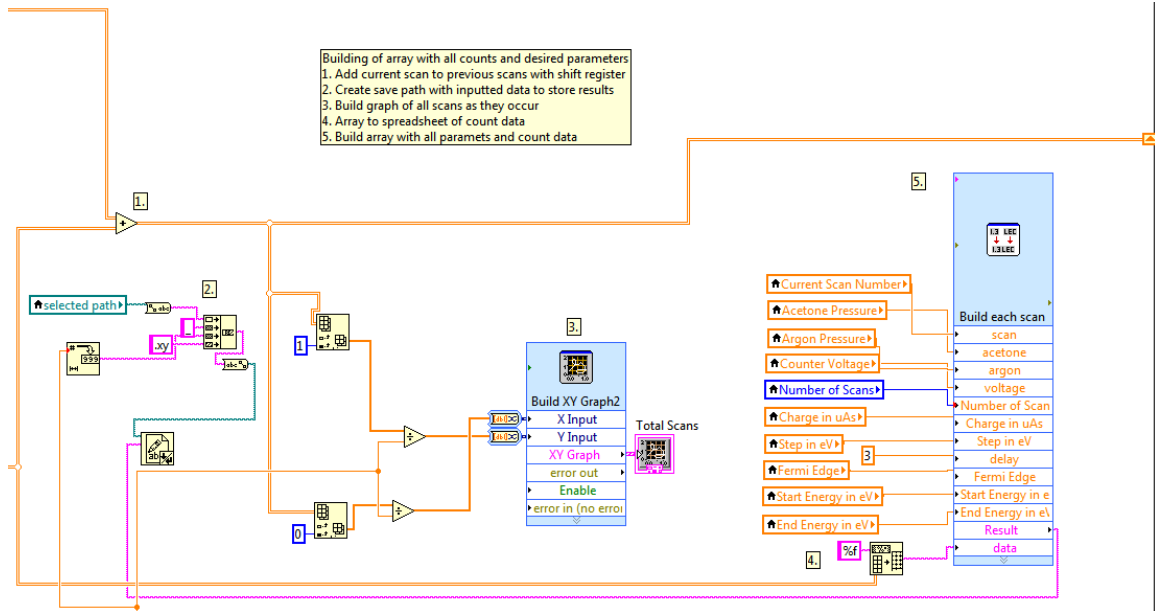


Figure 38: Array build for final output that is saved to .xy file.

Through the use of shift registers the count data for a full scan is saved and then added to the next scan. This is done for two reasons. First, while the scans are in process there is another graph which shows the average of the scans at that point. The second reason is that at the end there is another save file that contains the averaged scan information to avoid having the user do this manually.

The output from the array built in the previous figure is shown in Figure 39. All of the parameters noted are listed at the top of the file with a # sign designating a comment. This information is saved along with the data as a backup should anything happen to the original written notes. The file can also be analyzed with ease and compared to other scans. The output format carries a .xy extension where a special macro was written to extract the data into the software, Igor Pro. Igor Pro is a scientific and engineering data analysis program, which can produce publication quality graphs.

```

# Group: IPES_1
#
# Region:
# Analysis Method:      IPES
# Analyzer:             Geiger Counter
# Acetone Pressure:     1.00
# Argon Pressure:       200.00
# Counter Voltage:      505
# Number of Scans:     4
# Charge:               20|
# Step Size:            0.100
# Delay:                3.0
# Fermi Edge: 0.00
# Start Energy:         2.00
# End Energy:           14.00
# Comment:
#
# cycle: 0, curve: 0
#
2.003000      541.000000
2.103000      592.000000
2.203000      609.000000
2.303000      638.000000
2.404000      402.000000
2.504000      630.000000
2.604000      400.000000
2.704000      489.000000
2.804000      488.000000
2.904000      440.000000
3.005000      413.000000
3.005000      463.000000
3.105000      509.000000
3.305000      458.000000
3.405000      455.000000
3.500000      421.000000
3.606000      341.000000
3.706000      432.000000
3.806000      506.000000
3.906000      491.000000
4.007000      580.000000
4.106000      597.000000
4.207000      590.000000
4.307000      767.000000
4.407000      676.000000
4.507000      912.000000
4.608000      1057.000000
4.708000      1284.000000
4.808000      1409.000000
4.908000      2061.000000
5.008000      2318.000000
5.108000      2308.000000
5.209000      2783.000000
5.309000      2919.000000
5.409000      3258.000000
5.509000      3404.000000
5.610000      3267.000000
5.709000      3060.000000
5.810000      3398.000000
5.910000      3636.000000
5.910000      3359.000000

```

Figure 39: Sample output .xy data file.

CHAPTER 5: EXPERIMENTAL IPES SCANS AND CONCLUSION

5.1 Experimental Resolution of Detector

After successful completion of the setup and LabVIEW software, the system was tested to determine the resolution. An Ar^+ sputtered polycrystalline Au sample was inserted into the chamber for analysis. The scan was acquired using the parameters detailed in Appendix D. Figure 40 features the Fermi edge of the Au sample for resolution analysis. Due to analyzer broadening the resolution is required to later correct values in the determination of unoccupied state locations and the CBM of a sample. By fitting a line to the Fermi edge increase and drawing horizontal markers for the minimum and maximum, the resolution of the system can be acquired. Overall width of the edge is 0.86 eV and the resolution is therefore taken as half of the width, 0.43 eV. This value agrees well with the detector resolution expected from Chapter 3 and published data by Budke et al. [37].

The resolution analysis leads to the computation of the Fermi edge at 4.89 eV. After the assessment of the Fermi edge, the energy scale is adjusted according to convention by designating the Fermi edge to be 0 eV. The energy of the Fermi edge is independent of the sample measured due to the electrical contact between e-gun filament and sample. It only depends on the difference between the photon detector energy and the work function of the material used to generate electrons. From Chapter 3, the photon

detector has a minimum ionization energy of 9.7 eV and the work function of the tantalum disc used to generate electrons is ~ 4.25 eV [42]. The calculated energy difference of 5.35 eV is close to the experimental value 4.89 eV where the shift is accounted for by the tantalum disc energy spread of ≤ 0.7 eV [43].

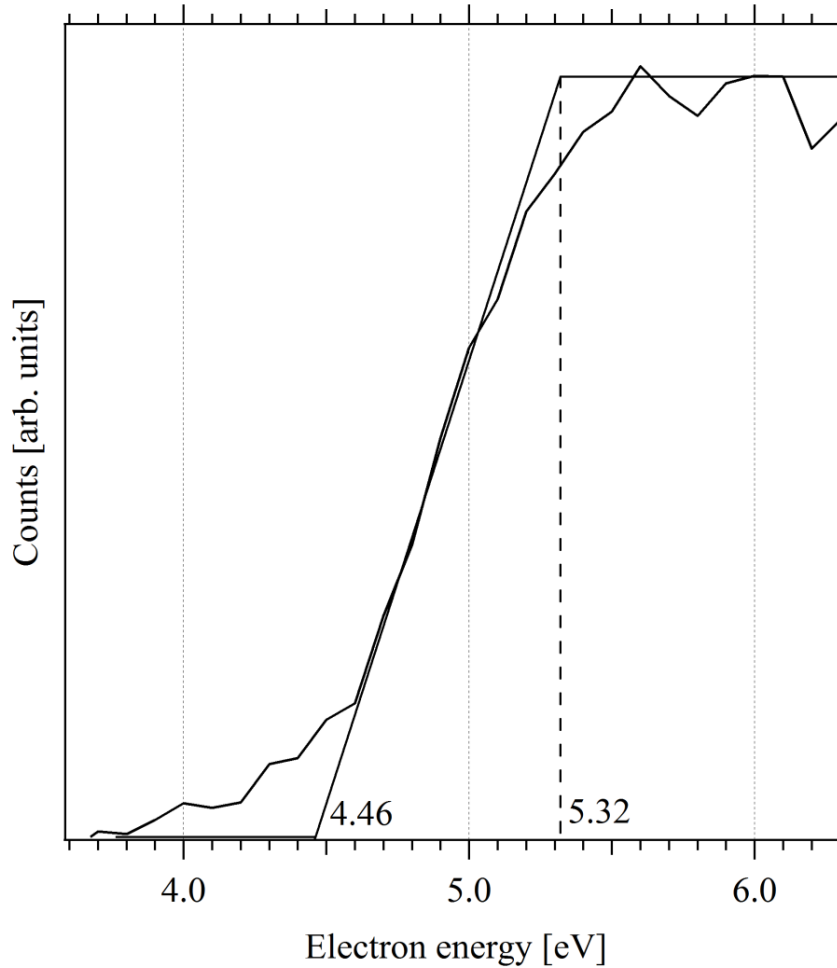


Figure 40: Sputtered Au measurement used to determine resolution of system.

The complete IPES scan of the polycrystalline Au is shown in Figure 41. The x-axis energy range has been changed to reflect the position of the Fermi edge. Its spectrum is very similar to IPES measurements of Au by Michel and Ferrer, and exhibits the same feature and shape [44]. This calibration scan will serve as a comparison for other materials whose transfer gap is unknown.

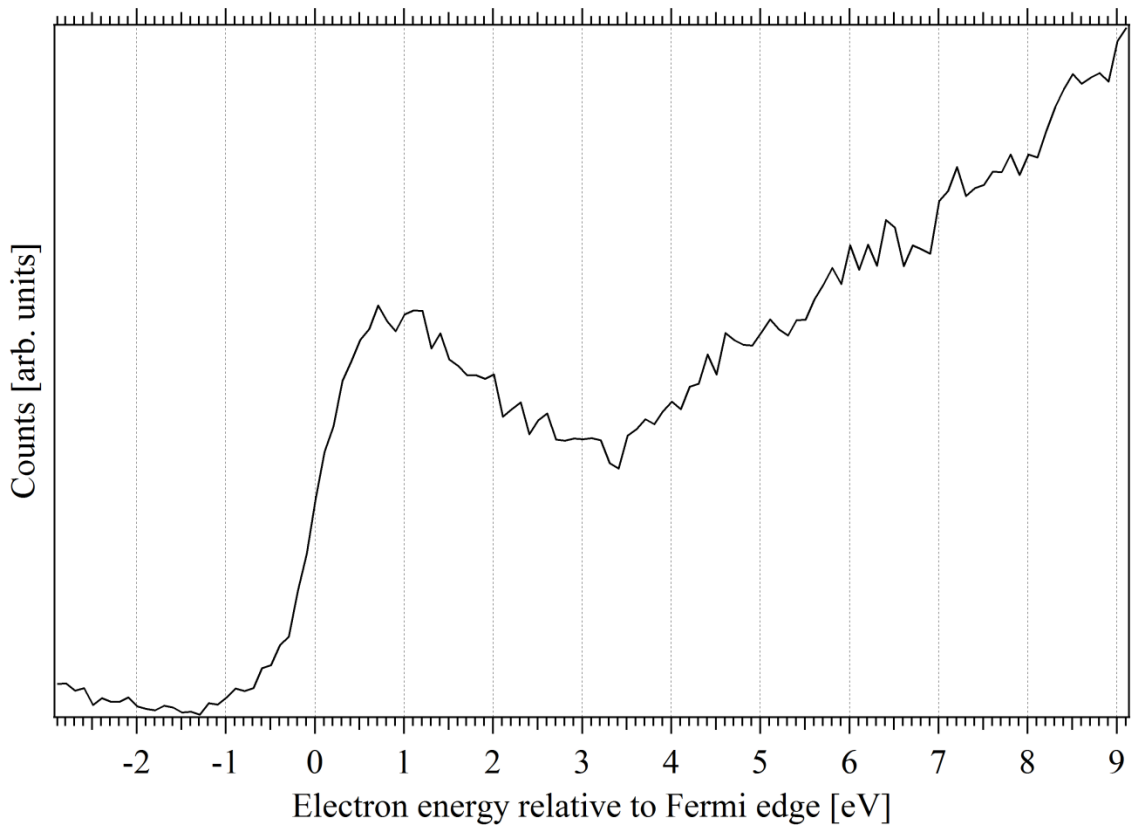


Figure 41: IPES scan of Au.

5.2 IPES Scan of Indium Tin Oxide (ITO)

Shown in Figure 42 is an IPES scan of indium tin oxide (ITO). ITO is a transparent conductive oxide commonly used in electronic devices such as touchscreens,

liquid crystal displays and electronic ink. The optical band gap for ITO ranges from 3.5 – 4.3 eV as published by Kim et al. [45]. The valence band maximum of ITO determined by UPS has been published as 3.25 eV by Gutmann et al. [46].

Utilizing the IPES scan of ITO, the CBM is acquired by investigating the conduction band onset and adjusting for detector broadening attained in Section 5.1. Using the resolution value of 0.43 eV, the CBM is established at 1.70 eV. This is indicated in the shifted line of Figure 42. In conjunction with the published VBM, the resulted transfer gap is 4.95 eV. From the discussion in Section 1.3 of the variation between optical band gaps and transfer gaps, the resultant ITO transfer gap corresponds well and is considerably larger than the optical gap.

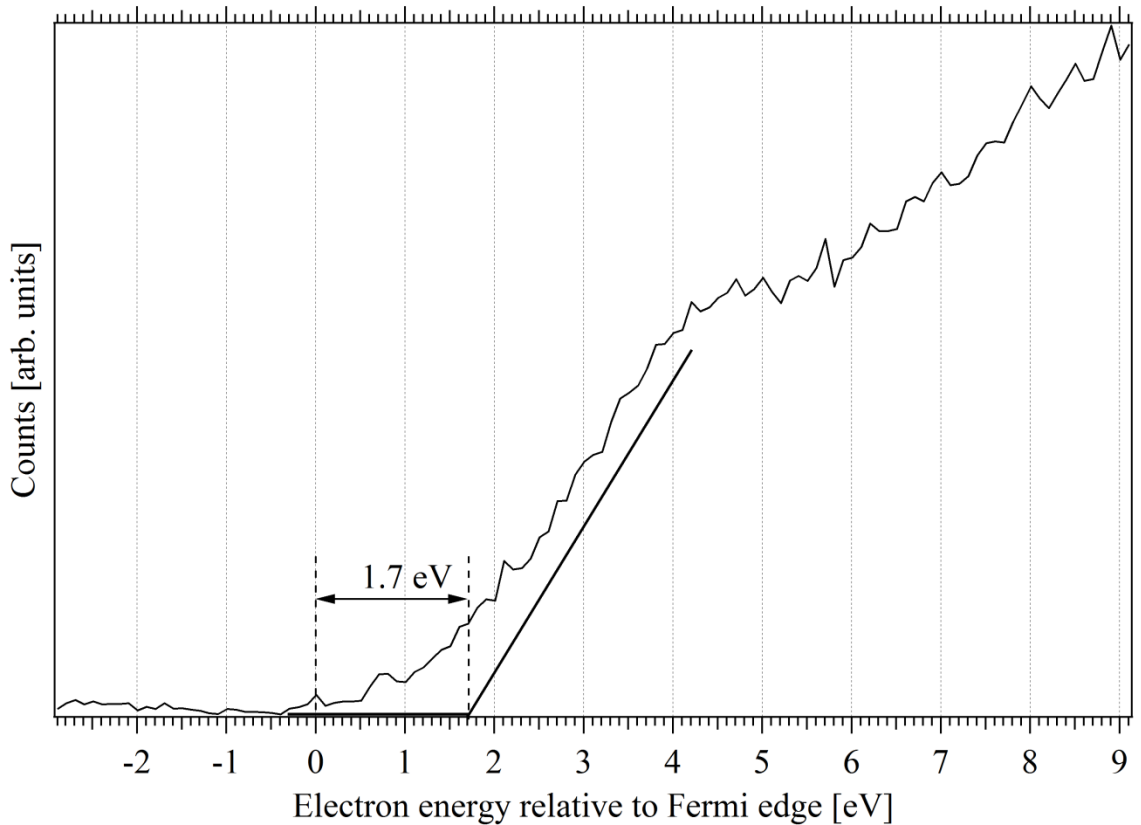


Figure 42: IPES scan of ITO showing a shift in the conduction band.

5.3 Conclusion

Inverse photoemission spectroscopy has been implemented as a method of studying the unoccupied states of materials. IPES measures the energy range between the Fermi energy E_F and the vacuum level E_{vac} . This thesis has detailed the physical construction of the components in the setup along with the software written to control operation. Background theory was introduced for both photoemission and inverse photoemission spectroscopy with examples of each.

The photon detector bandpass elements were explained and the combination of window/gas mixture required for a nominal resolution while conserving the count rate was discussed. The photon detector was examined with various gas mixtures where the optimal mixture chosen for scan repeatability was a partial acetone pressure of 1 mbar (N_2 calibration factor) and total acetone and argon pressure of 200 mbar (Ar calibration factor). The setup was tested with a known measurement of Au to determine both the experimental resolution of the detector and the location of the Fermi edge. This Fermi edge position will be utilized in all future measurements to quantify unoccupied state locations and the conduction band onset.

Further applications of this setup are promising. The IPES technique can be applied to many materials and interfaces. The ITO sample analyzed in Section 5.2 is only one such example where the conduction band minimum has been determined and is then utilized for transfer gap analysis. Interfaces between different materials can be analyzed as well and the band offset can be determined giving information about the electron and hole injection barriers when used in conjunction with UPS.

REFERENCES

1. Bonzel, H.P. and C. Kleint, *On the History of Photoemission*. Progress in Surface Science, 1995. **49**(2): p. 107-153.
2. Bracker, C., et al., *The photoelectric effect in external fields*. Physics Letters, 2005. **A**(347): p. 62-66.
3. Keller, O., *Chapter 3 Historical papers on the particle concept of light*, in *Progress in Optics*, E. Wolf, Editor 2007, Elsevier. p. 51-95.
4. Millikan, R.A., *Einstein's Photoelectric Equation and Contact Electromotive Force*. Physical Review, 1916. **7**(1): p. 18-32.
5. Reinert, F. and S. Hufner, *Photoemission spectroscopy-from early days to recent applications*. New Journal of Physics, 2005. **7**(97): p. 1-34.
6. Spicer, W.E. and C.N. Berglund, *d Band of Copper*. Physical Review Letters, 1964. **12**(1): p. 9-11.
7. Feibelman, P.J. and D.E. Eastman, *Photoemission spectroscopy--Correspondence between quantum theory and experimental phenomenology*. Physical Review B, 1974. **10**(12): p. 4932-4947.
8. Schaich, W.L., et al., *Photoemission in Solids I General Principles*1978: Springer-Verlag. 290.
9. Tanuma, S., C.J. Powell, and D.R. Penn, *Calculations of electron inelastic mean free paths*. Surface and Interface Analysis, 2004. **37**(1): p. 1-14.
10. Zangwill, A., *Physics at Surfaces*1988: Cambridge University Press. 454.
11. Hufner, S., *Photoelectron Spectroscopy: Principles and Applications*. 3rd ed2003: Springer. 662.
12. Schlaf, R., *Calibration of Photoemission Spectra and Work Function Determination*, University of South Florida. p. 1-4.

13. Liu, G., et al., *XPS and UPS Characterization of the TiO₂/ZnPcGly Heterointerface: Alignment of Energy Levels*. Journal of Physical Chemistry B, 2002. **106**(23): p. 5814-5819. doi:10.1021/jp014192b.
14. Dose, V. and G. Reusing, *Electron-Hole Pair Production and the Structure of Ultraviolet Isochromats*. Applied Physics, 1980. **23**: p. 131-134.
15. Roentgen, W.C., *On a New Kind of Rays*. Physik. Med. Ges., 1895. **137**(1): p. 1-29.
16. Duane, W. and F.L. Hunt, *On X-Ray Wave-Lengths*. Physical Review, 1915. **6**(2): p. 166-172.
17. Smith, N.V., *Inverse Photoemission*. Reports on Progress in Physics, 1988. **51**(9): p. 1227-1294.
18. Pendry, J.B., *Theory of inverse photoemission*. Journal of Physics C: Solid State Physics, 1981. **14**(9): p. 1381-1391.
19. Woodruff, D.P. and T.A. Delchar, *Modern Techniques of Surface Science*. 2nd ed1994: Cambridge University Press. 608.
20. Himpsel, F.J. and T. Fauster, *Probing valence states with photoemission and inverse photoemission*. Journal of Vacuum Science and Technology A, 1984. **2**(2): p. 815-821.
21. Himpsel, F.J., *Inverse Photoemission: Fundamentals and Applications to Semiconductors*. Physica Scripta, 1990. **1990**(T31): p. 171-178. doi:10.1088/0031-8949/1990/T31/024.
22. Shukla, A.K., S. Banik, and S.R. Barman, *Fabrication of an inverse photoemission spectrometer to study unoccupied electronic states*. Current Science, 2006. **90**(4): p. 490-496.
23. Cahen, D., A. Kahn, and E. Umbach, *Energetics of molecular interfaces*. Materials Today, 2005. **8**(7): p. 32-41.
24. Geiger, H. and W. Mueller, *Elektronenzaehlrrohr zur Messung schwachster Aktivitaeten (Electron counting tube for the measurement of the weakest radioactivities)*. Die Naturwissenschaften, 1928. **16**(31): p. 617-618.
25. Denninger, G., V. Dose, and H. Scheidt, *A VUV isochromat spectrometer for surface analysis*. Applied Physics A: Materials Science and Processing, 1979. **18**(4): p. 375-380.

26. Dose, V., *Study of empty electronic states by inverse ultraviolet photoemission*. Journal of Physical Chemistry, 1984. **88**(9): p. 1681-1690.
27. Knoll, G.F., *Radiation Detection and Measurement*. 2nd ed 1989: John Wiley and Sons, Inc.
28. Sahin, O., et al., *Penning transfer in argon-based gas mixtures*. Journal of Instrumentation, 2010. **5**(5): p. 1-30.
29. Bronic, I.K. and B. Grosswendt, *Comparative study of gas amplification and energy resolution in some argon-based mixtures*. Nuclear Instruments and Methods in Physics Research B, 2000. **168**: p. 437-447.
30. Murphy, E.L. and R.H. Good, Jr., *Thermionic Emission, Field Emission, and the Transition Region*. Physical Review, 1956. **102**(6): p. 1464-1473.
31. Gilmour, A.S., *Klystrons, Traveling Wave Tubes, Magnetrons, Cross-Field Amplifiers, and Gyrotrons* 2011: Artech House.
32. Physics, K., *ELG-2 / EGPS-1022 Electron Gun and Power Supply System Manual*, 2009.
33. Prince, K.C., *Improved inverse photoemission detector*. Review of Scientific Instruments, 1988. **59**(5): p. 741-742.
34. Hill, I.G. and A.B. McLean, *A comparison of two high performance inverse photoemission bandpass detectors*. Review of Scientific Instruments, 1998. **69**(1): p. 261-264.
35. Schedin, F., G. Thornton, and R.I.G. Uhrberg, *Windows and photocathodes for a high resolution solid state bandpass ultraviolet photon detector for inverse photoemission*. Review of Scientific Instruments, 1996. **68**(1): p. 41-46.
36. Heath, D.F. and P.A. Sacher, *Effects of a Simulated High-Energy Space Environment on the Ultraviolet Transmittance of Optical Materials between 1050 and 3000 Angstroms*. Applied Optics, 1966. **5**(6): p. 937-943.
37. Budke, M., et al., *Inverse photoemission with energy resolution better than 200 meV*. Review of Scientific Instruments, 2007. **78**(8).
38. Maniraj, M., et al., *High energy resolution bandpass photon detector for inverse photoemission spectroscopy*. Review of Scientific Instruments, 2011. **82**(9).
39. Dibeler, V.H., et al., *Effect of hot bands on the ionization threshold of some diatomic halogen molecules*. International Journal of Mass Spectrometry and Ion Physics, 1971. **7**(3): p. 209-219.

40. Trott, W.M., N.C. Blais, and E.A. Walters, *Molecular beam photoionization study of acetone and acetone-d₆*. Journal of Chemical Physics, 1978. **69**(7): p. 3150-3158. doi:10.1063/1.437009.
41. Funnemann, D. and H. Merz, *10 eV photon detector for inverse photoemission*. Journal of Physics E: Scientific Instruments, 1986. **19**(7): p. 554-557. doi:10.1088/0022-3735/19/7/011.
42. *CRC Handbook of Chemistry and Physics*. 89 ed.
43. Physics, K., *Tantalum Disc Cathodes: Thermionic Emitters*.
44. Michel, E.G. and S. Ferrer, *Empty Interface State in Pt/Au(001) Revealed by Inverse Photoemission*. Europhysics Letters, 1987. **4**(5): p. 603-608.
45. Kim, H., et al., *Electrical, optical, and structural properties of indium--tin--oxide thin films for organic light-emitting devices*. Journal of Applied Physics, 1999. **86**(11): p. 6451-6461.
46. Gutmann, S., et al., *Electronic structure of indium tin oxide/nanocrystalline TiO₂ interfaces as used in dye-sensitized solar cell devices*. Journal of Applied Physics, 2011. **109**(11): p. 113719-10.

APPENDICES

Appendix A: Filling the Detector with Gas

The gas mixture inside the photon detector is very important and any impurities can change its behavior. Before filling the photon detector with the gas mixture, the detector has to be completely evacuated. The gas manifold is opened in such a way that the turbomolecular pump is pumping only the photon detector. Referring to Figure 14 on page 26, the valve to the pump is slowly opened due to the fact that the pump cannot handle higher pressures than 10^{-4} torr. Heat tape is wrapped around the detector to accelerate the outgassing of any molecules in the tube by heating to 100 °C.

Once the detector has been pumped down and is below 10^{-3} mbar range as measured by the thermovac gauge, the gas can then be let into the detector one at a time. Before opening the acetone valve it is essential to make sure the turbomolecular pump valve is closed. Referring to Figure 14, only the valve to the photon detector is opened. The acetone valve is very slowly opened and the pressure is read on the thermovac gauge with the N₂ calibration factor. Once the reading hits the 1 mbar acetone partial pressure the valve is closed. The detector valve is still left open. During this time the argon cylinder is opened for a few seconds at the main valve on the bottle to fill up the line before the first valve. Note that the pressure in this small line will be very high. The first valve is then opened fully. Following the line towards the photon detector, the second valve is then very carefully opened. The pressure reading should be changed to Ar for the total combination pressure. Since the line will be at an overpressure coming from the argon cylinder there is no leaking of the acetone out of the line previously filled.

Appendix A (Continued)

When the total pressure reaches 200 mbar, the second valve can be closed. The valve to the photon detector can also be closed. The gas should then settle for 20 minutes before a scan is started. While waiting for the gas to settle, the electron gun can be started and warmed up. The warming process is explained in detail in Appendix B.

The remaining valves of the manifold can then be opened for pumping out the lines to ensure a high vacuum when refilling the counter. Note again to slowly open the turbomolecular pump valve because the lines now have high pressure due to the argon previously released. The gas mixture in the photon detector can now be used for up to two weeks without refilling.

Appendix B: Starting Up the Electron Gun

The electron gun has to be carefully ramped up to operating conditions otherwise its lifetime can be drastically reduced. Looking at Figure 27 in Section 4.2, there are 3 very important parameters when powering on the electron gun.

First the cathode element has to be heated to operate in between the temperature and space charge limited modes described in the electron gun theory section of Chapter 1. The source voltage is slowly raised by increments of 0.25 V. As the voltage increases there will be a graphical indicator of the temperature increasing. This is determined by the current flowing through the tantalum disc. As the disc heats up its resistivity will change. The current will drop and this is reflected in the temperature shown in the graph of the Kimball software in Figure 43. The source voltage should initially be increased so as the cathode temperature is 2000 °K. Then the user must wait approximately 20 minutes and occasionally check the current flowing through the cathode. The source voltage must again be increased to raise the now lowered current and temperature. After this time the source voltage will be ~ 1.55 V for a current of 1.6 A.

The second part of preparing the electron beam is to set the desired electron energy. For startup the energy is set to the default lowest value in the IPES software (2 eV). The electron energy is set through the potential difference between the cathode and first anode. When the electron beam leaves the floating region of the gun and approaches the grounded aperture, its acceleration is varied by the relative voltage difference between the energy supply and the 1st anode voltage. Without applying a 1st anode voltage the electron is not accelerated in the gun and no current is measured.

Appendix B (Continued)

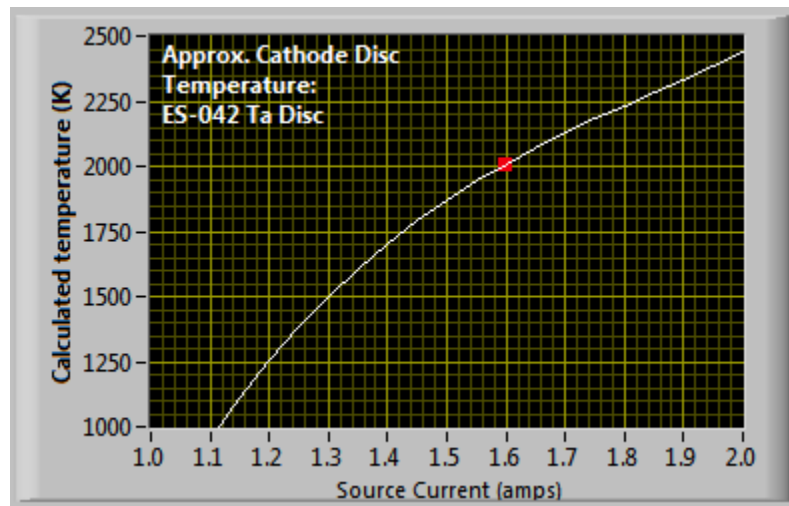


Figure 43: Electron gun cathode temperature vs. current.

Lastly the 1st anode voltage is increased. While there is no software safeguard to the rate of increase in this parameter, maximum 20 V increments are recommended. The operating value of the G2 voltage is 60 V. There should now be an emission current measured and displayed on the Kimball software around 9 μ A.

Appendix C: Setting Up Electronics

The preamplifier is connected directly to the photon detector through its front output. On the back of the preamplifier is an input for the high voltage from the Stanford power supply and an output to amplifier. The preamplifier connects to the back of the amplifier for a power source. This is one way to reduce noise and have the components share a ground source. The amplifier is set up with the following specifications:

- Coarse gain = 50
- Fine gain = 0.5
- Shaping time = 3.0 μ s
- Output range = +10 V
- Base line restoration = OUT
- Delay = OUT
- Polarity = NEG

The amplifier output is fed into the single channel analyzer (SCA). The value for the lower level cutoff in the SCA is 0.40 V with $\Delta = 10$ V. The lower level can be tested by viewing the LED on the front of the SCA. If the signal level is high enough to produce a positive output then the light will blink for each instance.

The high voltage is finally turned on and the “Detector voltage scan” mode in the IPES software is utilized. The scan is started with start and end voltages set to 500 V and 650 V, respectively, with a step size of 5 V. After the scan is finished, a voltage slightly

Appendix C (Continued)

below the maximum is chosen, ~ 5 to 10 V below the highest count rate. The applied voltage is kept steady during IPES scanning.

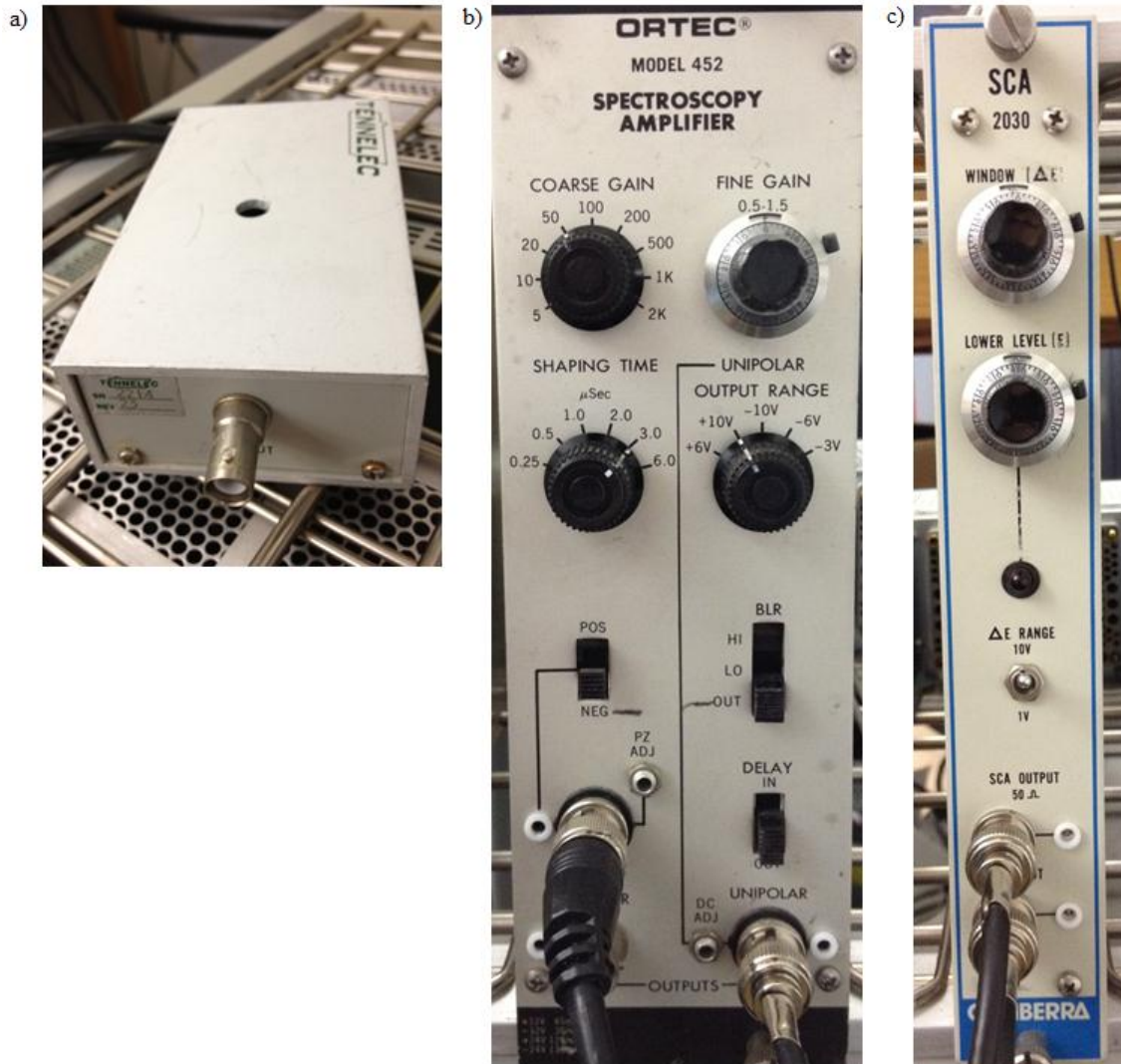


Figure 44: a) The preamplifier, b) amplifier and c) single channel analyzer component images.

Appendix D: Starting a Measurement

The operating parameters have to be input in the IPES LabVIEW software.



Values used for the scans of Au in characterizing the system were:


- Start energy = 2 eV
- End energy = 14 eV
- Step size = 0.10 eV
- Charge in μAs = 40
- Number of scans = 4

After the data is set then the user can press “Start Measurement” in the automatic mode. A popup window will appear to have the user select a save path and file name. Note that the filename should be left without an extension at the end. The program will automatically add the scan number to the end of the file name and make it a .xy file. Once the scans are finished a pop up message will appear saying the measurement is done. Afterwards, the saved data files can be found in selected path. The files can be imported through the Igor Pro macro for IPES.

Appendix E: Copyright Permissions

E.1 Permission for Use of Figure 4

HomeCreate AccountHelp



ACS Publications Title: XPS and UPS Characterization of the TiO₂/ZnPcGly Heterointerface: Alignment of Energy Levels
High quality. High impact.

Author: Guangming Liu et al.

Publication: The Journal of Physical Chemistry B

Publisher: American Chemical Society

Date: Jun 1, 2002

Copyright © 2002, American Chemical Society

User ID

Password

Enable Auto Login

[Forgot Password/User ID?](#)

If you're a [copyright.com](#) user, you can login to RightsLink using your [copyright.com](#) credentials. Already a [RightsLink](#) user or want to [learn more?](#)

PERMISSION/LICENSE IS GRANTED FOR YOUR ORDER AT NO CHARGE

This type of permission/license, instead of the standard Terms & Conditions, is sent to you because no fee is being charged for your order. Please note the following:

- Permission is granted for your request in both print and electronic formats, and translations.
- If figures and/or tables were requested, they may be adapted or used in part.
- Please print this page for your records and send a copy of it to your publisher/graduate school.
- Appropriate credit for the requested material should be given as follows: "Reprinted (adapted) with permission from (COMPLETE REFERENCE CITATION). Copyright (YEAR) American Chemical Society." Insert appropriate information in place of the capitalized words.
- One-time permission is granted only for the use specified in your request. No additional uses are granted (such as derivative works or other editions). For any other uses, please submit a new request.

Copyright © 2012 [Copyright Clearance Center, Inc.](#) All Rights Reserved. [Privacy statement.](#)
Comments? We would like to hear from you. E-mail us at customercare@copyright.com

Appendix E (Continued)

E.2 Permission for Use of Figure 6



Ervin Gina <ervman1@gmail.com>

Permission

1 message

office@ias.ernet.in <office@ias.ernet.in>
To: ervman1@gmail.com

Tue, May 15, 2012 at 5:12 AM

Dear Ms Gina,

Thank you for your mail seeking permission to reproduce figure from the article: "Fabrication of an inverse photoemission spectrometer to study unoccupied electronic states" by Shukla, A.K. et al., published in Current Science, 90(4), 490-496, 2006.

We hereby grant you permission to reproduce this figure in your thesis entitled "Implementation and optimization of an inverse photoemission spectroscopy setup".

We urge you to keep the author also informed.

Please make sure that the source of the figure is acknowledged properly.

Regards,
C.S. Ravi Kumar

Appendix E (Continued)

E.3 Permission for Use of Figure 7



To: permissions@iop.org,
Cc:
Bcc:
Subject: Figure permission
From: Ervin Gina <ervman1@gmail.com> - Tuesday 29/05/2012 17:21

05/29/2012

To whom it may concern,

I am currently working on my masters thesis entitled "Implementation and optimization of an inverse photoemission spectroscopy setup". I would like to use a figure in an article published in Physica Scripta.

Figure 7. Himpsel, F.J., *Inverse Photoemission: Fundamentals and Applications to Semiconductors*. Physica Scripta, 1990. 1990(T31): p. 171-178.

This is non profit and proper referencing of the article will be done.

In case you do not control these rights, I would appreciate it if you could let me know to whom I should apply for permissions.

Thank you,

Ervin Gina

PERMISSION TO REPRODUCE AS REQUESTED IS GIVEN PROVIDED THAT:

- (a) the consent of the author(s) is obtained
- (b) the source of the material including author, title of article, title of journal, volume number, issue number (if relevant), page range (or first page if this is the only information available), date and publisher is acknowledged.
- (c) for material being published electronically, a link back to the original article should be provided (via DOI).

IOP Publishing Ltd
Temple Circus
Temple Way
BRISTOL
BS1 6BE

31/05/2012
Date

.....
Rights & Permissions \

Appendix E (Continued)

Franz Himpel fhimpel@facstaff.wisc.edu

to me ▾

I am happy to grant permission.

With best regards,

Franz Himpel

...

...

Content-type: application/octet-stream; name="Gina 31 05.pdf"

Content-disposition: attachment; filename="Gina 31 05.pdf"

X-Attachment-Id: 3550017567107eec_0.1

Franz J. Himpel

Physics Dept., University of Wisconsin Madison

<http://uw.physics.wisc.edu/~himpel/>

Appendix E (Continued)

E.4 Permission for Use of Figure 18

AMERICAN INSTITUTE OF PHYSICS LICENSE TERMS AND CONDITIONS

Apr 30, 2012

License Number	2899090430300
Order Date	Apr 30, 2012
Publisher	American Institute of Physics
Publication	Journal of Chemical Physics
Article Title	Molecular beam photoionization study of acetone and acetone-d6
Author	Wayne M. Trott, Normand C. Blais, Edward A. Walters
Online Publication Date	Oct 1, 1978
Volume number	69
Issue number	7
Type of Use	Thesis/Dissertation
Requestor type	Student
Format	Electronic
Portion	Figure/Table
Number of figures/tables	1
Title of your thesis / dissertation	Implementation and optimization of an inverse photoemission spectroscopy setup
Expected completion date	Aug 2012
Estimated size (number of pages)	100
Total	0.00 USD
Terms and Conditions	

American Institute of Physics -- Terms and Conditions: Permissions Uses

American Institute of Physics ("AIP") hereby grants to you the non-exclusive right and license to use and/or distribute the Material according to the use specified in your order, on a one-time basis, for the specified term, with a maximum distribution equal to the number that you have ordered. Any links or other content accompanying the Material are not the subject of this license.

1. You agree to include the following copyright and permission notice with the reproduction of the Material: "Reprinted with permission from [FULL CITATION]. Copyright [PUBLICATION YEAR], American Institute of Physics." For an article, the copyright and permission notice must be printed on the first page of the article or book chapter. For photographs, covers, or tables, the copyright and permission notice may appear with the Material, in a footnote, or in the reference list.

Appendix E (Continued)

2. If you have licensed reuse of a figure, photograph, cover, or table, it is your responsibility to ensure that the material is original to AIP and does not contain the copyright of another entity, and that the copyright notice of the figure, photograph, cover, or table does not indicate that it was reprinted by AIP, with permission, from another source. Under no circumstances does AIP, purport or intend to grant permission to reuse material to which it does not hold copyright.
3. You may not alter or modify the Material in any manner. You may translate the Material into another language only if you have licensed translation rights. You may not use the Material for promotional purposes. AIP reserves all rights not specifically granted herein.
4. The foregoing license shall not take effect unless and until AIP or its agent, Copyright Clearance Center, receives the Payment in accordance with Copyright Clearance Center Billing and Payment Terms and Conditions, which are incorporated herein by reference.
5. AIP or the Copyright Clearance Center may, within two business days of granting this license, revoke the license for any reason whatsoever, with a full refund payable to you. Should you violate the terms of this license at any time, AIP, American Institute of Physics, or Copyright Clearance Center may revoke the license with no refund to you. Notice of such revocation will be made using the contact information provided by you. Failure to receive such notice will not nullify the revocation.
6. AIP makes no representations or warranties with respect to the Material. You agree to indemnify and hold harmless AIP, American Institute of Physics, and their officers, directors, employees or agents from and against any and all claims arising out of your use of the Material other than as specifically authorized herein.
7. The permission granted herein is personal to you and is not transferable or assignable without the prior written permission of AIP. This license may not be amended except in a writing signed by the party to be charged.
8. If purchase orders, acknowledgments or check endorsements are issued on any forms containing terms and conditions which are inconsistent with these provisions, such inconsistent terms and conditions shall be of no force and effect. This document, including the CCC Billing and Payment Terms and Conditions, shall be the entire agreement between the parties relating to the subject matter hereof.

This Agreement shall be governed by and construed in accordance with the laws of the State of New York. Both parties hereby submit to the jurisdiction of the courts of New York County for purposes of resolving any disputes that may arise hereunder.

If you would like to pay for this license now, please remit this license along with your payment made payable to "COPYRIGHT CLEARANCE CENTER" otherwise you will be invoiced within 48 hours of the license date. Payment should be in the form of a check or money order referencing your account number and this invoice number RLNK500770718.

**Copyright Clearance Center
Dept 001
P.O. Box 843006
Boston, MA 02284-3006**

Appendix E (Continued)

E.5 Permission for Use of Figure 19



To: permissions@iop.org,
Cc:
Bcc:
Subject: Figure permission
From: Ervin Gina <ervman1@gmail.com> - Tuesday 01/05/2012 21:49

05/01/2012

To whom it may concern,

I am currently working on my masters thesis entitled "Implementation and optimization of an inverse photoemission spectroscopy setup". I would like to use a figure in an article published in the Journal of Physics E: Scientific Instruments.

Figure 1, "10 eV photon detector for inverse photoemission." D. Funnemann and H. Merz. Journal of Physics E: Scientific Instruments 19(7): 554-557. (1986)

In case you do not control these rights, I would appreciate it if you could let me know to whom I should apply for permissions.

Thank you,

Ervin Gina

Research Assistant

University of South Florida

PERMISSION TO REPRODUCE AS REQUESTED IS GIVEN PROVIDED THAT:

(a) the consent of the author(s) is obtained

(b) the source of the material including author, title of article, title of journal, volume number, issue number (if relevant), page range (or first page if this is the only information available), date and publisher is acknowledged.

(c) for material being published electronically, a link back to the original article should be provided (via DOI).

IOP Publishing Ltd

Temple Circus

Temple Way

BRISTOL

BS1 6BE

03/05/2012
Date

.....
Rights & Permissions